

NASA CR-

147400

Photo Data Analysis S-221

NASA Contract NAS 9-13196

GEOLOGIC STRUCTURE OF SHALLOW MARIA

Rene' A. De Hon, Principal Investigator

John A. Waskom, Co-Investigator

(NASA-CR-147400) GEOLOGIC STRUCTURE OF
SHALLOW MARIA (Arkansas Univ., Monticello.)
96 p HC \$5.00 CSCI 03B

N76-17001

Unclas
63/91 09970

University of Arkansas at Monticello
Monticello, Arkansas

December 1975

Photo Data Analysis S-221

NASA Contract NAS 9-13196

GEOLOGIC STRUCTURE OF SHALLOW MARIA

Rene' A. De Hon, Principal Investigator

John A. Waskom, Co-Investigator

University of Arkansas at Monticello
Monticello, Arkansas

December 1975

ABSTRACT

Isopach maps and structural contour maps of the eastern mare basins (30°N to 30°S ; 0° to 100°E) are constructed from measurements of partially buried craters. The data, which are sufficiently scattered to yield gross thickness variations, are restricted to shallow maria with less than 1500-2000 m of mare basalts. The average thickness of basalt in the irregular maria is between 200 and 400 m.

Multiringed mascon basins are filled to various levels. The Serenitatis and Crisium basins have deeply flooded interiors and extensively flooded shelves. Mare basalts in the Nectaris basin fill only the innermost basin, and mare basalts in the Smythii basin occupy a small portion of the basin floor. Sinus Amoris, Mare Spumans, and Mare Undarum are partially filled troughs concentric to large circular basins. The Tranquillitatis and Fecunditatis are composite depressions containing basalts which flood degraded circular basins and adjacent terrain modified by the formation of nearby circular basins.

Correlations between surface topography, basalt thickness, and basin floor structure are apparent in most basins. The mare surface is commonly depressed in regions of thick mare basalts; mare ridges are typically

located in regions of pronounced thickness changes; and arcuate mare rilles are confined to thin mare basalts. Most surface structures are attributed to shallow stresses developed within the mare basalts during consolidation and volume reduction.

INTRODUCTION

Purpose and Scope

The mare basalts and the basins which contain them exhibit a diversity of surface shapes, sizes, and forms. Designation of maria as circular, multiringed, or irregular has important implications for the origin of the basins and the lunar processes operating to modify them after formation. Isopach maps of the mare basalts and reconstructions of the paleotopography prior to emplacement of the basalt provide important data bases for the description and study of mare materials and the basins in which they are emplaced.

This paper presents a three-fold study of mare basalts. The major objectives are:

1. To estimate the thickness of mare basalts in the eastern maria and to construct isopach maps of the basalts.
2. To determine sub-basalt basin floor topography; hence, the configuration of the basins in which basalts have collected.
3. To identify and correlate topographic variations of the surface (large and small scale) with variations in basalt thickness or basin floor topography.

The area of investigation is limited to the eastern maria (30°N - 30°S ; 0° - 100°E). Within these limits there is a maximum of photographic and topographic data derived from the Apollo program. Further, the eastern maria provide a variety of surface features and basinal types with a limited size range.

The method of estimating thickness is restricted to crater geometric techniques. Other photogeologic or remote sensing methods may provide thickness data, but these methods are not, at this time, fully developed or they yield data distribution insufficient to be used alone. The addition of data from multiple sources will eventually provide a more refined description of mare basalt thickness.

Background

Baldwin (1949, 1963) demonstrated that for fresh terrestrial explosion craters, known meteor impact craters, and fresh lunar craters, there is an interdependency of rim height and interior depth with crater diameter. Baldwin's (1963) data for lunar ray craters take the form of a curvilinear plot on log-log coordinates. Pike (1967, 1972) re-evaluated the data from new crater measurements as two linear expressions on log-log coordinates (Fig. 1). The equations for external rim

heights of fresh lunar craters are:

$$h = 0.053D^{0.94} \quad D < 17.5 \text{ km}$$

$$h = 0.270D^{0.34} \quad D > 17.5 \text{ km}$$

where h is the height of the rim above the surrounding surface in km and D is the crater rim crest diameter in km.

Craters partially buried by mare basalts are recognized as rings or incomplete rings of non-mare material protruding above the mare basalt plains. Complete shallow burial results in "ghost rings" or "ghost craters" (Cruikshank *et al.*, 1973) with mare material draped over the submerged crater rim. Marshall (1963) and Eggelton (1963) used Baldwin's ratios of rim height to crater diameter to estimate the thickness of mare materials of Oceanus Procellarum in the Lansberg region of the Moon. DeHon (1974, 1975a) used Pike's data to construct isopach maps of Mare Tranquillitatis, Mare Nectaris, Mare Spumans, and Mare Undarum.

Method

Thickness estimates of mare basalts are based on the average depth of burial of pre-mare craters. The average diameter and rim ^{height} of partially buried craters within mare basins is determined from Lunar Topographic Orthophotographs. For partially buried craters, the

exposed rim height minus the original pre-burial rim height (determined from rim height to diameter ratios of fresh craters) is assumed to be the thickness of basalt in the area of the crater (Fig. 2). For completely buried craters, observed as ghost rings, the thickness is assumed to be equal to the calculated rim height of the buried crater. This estimate ignores local lensing of the crater interior and wedging around the crater rim. The result is that of obtaining a thickness estimate in the area of the crater with the local relief of the crater removed.

If a sufficient population and aerial distribution of buried craters exist throughout a basin, it is possible to obtain lateral variations in thickness and to construct an isopach map. The data distribution is necessarily scattered (Fig. 3), but it is sufficiently random to yield an overall thickness distribution except in areas where the thickness exceeds 1.5-2.0 km. For most buried craters the thickness estimate is plotted at the center of the crater (to the nearest 0.1° long. and lat.). For some large craters as many as three thickness estimates are plotted at rim crest locations. For a crater located near the edge of the maria, the thickness is determined and plotted for the rim crest projecting into the maria. Since craters occupy large

areas (5-50 km diameter) the thickness estimate at any one crater represents an average over a large area. . Abrupt variations in thickness can not be detected.

Isopach maps are produced using a contouring program on disk at the University of Arkansas Data Processing Center. Data points are identified by longitude, latitude, thickness of mare basalt, and average surface elevation (Append.). The data are used to generate a grid of thickness values, surface elevations or basin floor elevations (surface minus thickness). Contour or isopach lines were interpolated from the grid by second degree polynomial fitting. The grid interval and the number of data points used in the interpolation varied from basin to basin depending on the spacing of data points. Figures 4,5, and 6 are composite maps of all eastern mare basins.

Topographic information used in this study is derived primarily from Lunar Topographic Orthophotographs. Where Apollo stereographic coverage is not available, relative heights were taken from Lunar Aeronautic Charts. In western and southern Mare Tranquillitatis (Fig. 4) surface topography is derived from radar topographic charts (Zisk et al., 1974).

Limitations and Accuracy

Data points used in the construction of the isopach maps are necessarily limited to the uneven and scattered distribution of partially buried craters preserved within the mare basins. The contact between mare materials and terra materials defines the zero isopach line, provides constraint to possible models and provides control for thickness projections. A total of 622 data points (422 basin edge and 200 interior) are used in construction of the isopach map (Fig. 3). The distribution is roughly one sampling point per two square degrees. Data within the circular mascon basins is limited to the relatively shallow shelf areas. Craters are obscured as basalt thickness exceeds 1.5-2.0 km.

One check on the overall accuracy of the isopach map is provided by surface contouring. Surface topographic maps are constructed using only the elevation data at each thickness sampling point. The extent to which the reconstructed surface topography matches the topography of the LTO series provides a check on the ability of the limited data spacing to reproduce the surface topography or thickness distribution. The generalized surface maps do provide a reasonable reproduction of the gross surface features, however, the rather wide

spacing of sampling points does not allow retention of small surface features.

A second, and presently unevaluated, consideration in the accuracy of the isopach map is the state of preservation of buried craters and the extent to which they vary from the trend of the rim height-diameter equations. A number of processes modify craters (Head, 1974) including impact or ballistic erosion, slumping, isostatic adjustments, tectonism, and volcanism. Most of the processes of crater modification tend to increase the apparent diameter of the crater and decrease the rim height. As a result, the estimates of depth of burial tend to overestimate the actual thickness in the area of modified craters. Underestimation of basalt thickness may occur at localities of ghost craters with mare basalts draped over the buried rim. The extent to which a crater may be completely buried yet maintain surface expression is an unknown factor. In most basins, the buried craters are known to have formed after some major crater destruction event (i.e. deposition of ejecta derived from nearby circular mare); hence, the craters formed within rather discrete time intervals and may not have suffered severe degradation before deposition of mare basalts.

Alternate Methods

Several techniques could be applied to provide checks on existing thickness models, to add refinement to data distribution, or to serve as an alternate means of estimating basalt thickness. Not all of the techniques are necessarily developed to their fullest potential at this time. Methods which either are now applicable, or might be in the near future are reviewed in three major classes: stratigraphic-structural, geophysical, and remote sensing geochemical.

Stratigraphic-structural techniques - Some surface features of the mare basalts may be of structural origin and may provide thickness information. Spatial correlation of mare ridges and rilles indicates that the thickness of mare basalts or the configuration of the basin floor is a controlling factor in the location of these features. If certain restrictions are assumed for the mode of formation of these features, then quantitative estimates can be applied. If lunar arcuate rilles are analogous to some terrestrial graben (Baldwin, 1949; McGill, 1970), the width of the rille may be a function of the thickness of the mare basalts. If rilles in mare basalts form in response to tension in the basalt which

is essentially decoupled from the underlying rocks then the width of the graben formed is a function of the depth to the decollement zone. Similarly the geometry of concentric folding is related to the thickness of layers undergoing folding (DeSitter, 1956). If mare ridges are compressional fold features, their elevation and crustal shortening can be used to estimate the thickness of the layer being folded.

Crater statistical methods are not restricted to rim height-diameter relationships used in the present study. Partial burial of a crater results in a change in the rim crest to rim width ratio. A multivariant function of rim width, rim height, and crater diameter can be employed to determine depth of burial (Baldwin, 1970; Eggleton et al., 1974). This method provides a readily available means of estimating basalt thickness in regions where stereophotography or optimum sun angles do not allow accurate measurement of rim height. The data relating rim width to diameter display considerable scatter (Pike, 1974; McGetchin et al., 1974; Settle and Head, 1975); hence, a wider range of error is introduced into the estimates. Nevertheless, this technique will be important in the large areas of mare surfaces which do not contain adequate elevation data.

Geophysical techniques - Geophysical methods which provide information as to the thickness of mare basalts include lunar gravimetric measurements, seismic studies, and sounder profiling. Variations in the lunar gravity field as measured from changes in velocities of satellites in orbit allow structural and density modeling of the larger features of the Moon (Muller and Sjogren, 1968; Sjogren et al., 1972, 1974, 1975). A large variety of near surface structural and stratigraphic models have been proposed to account for the gravity anomalies (Baldwin, 1968; Kaula, 1969; Stripe, 1968; Urey, 1968; Wise and Yates, 1970; Howard, 1970; Scott, 1974; Scott et al., 1975). Continued tracking of lunar satellites in low orbits will greatly enhance the gravimetric data, and realistic models of mare basalt distribution may be tested and refined. Similarly, gross structure of the moon can be determined by passive seismometry (Latham et al., 1970; Toksoz, 1973; Kovach et al., 1973). However, detailed seismic profiling on the scale required for basin structures is not possible without a large number of surface stations. Structural information for the upper lunar crust is limited to generalized data or very localized thickness determinations. The lunar sounder experiment (Phillips et al., 1973) provides a capability of yielding continuous surface and

subsurface profiles to a depth of approximately 1000 meters. Data reduction and systematic noise make subsurface profiling difficult, but a subsurface profile of the eastern shelf of Mare Serenitatis has been obtained.

Remote sensing geochemical techniques - Remote sensing, whether by earth-based telescopic or satellite experiments have been employed to detect compositional variations in exposed lunar materials (McCord et al., 1972; Peters et al., 1975; Alder et al., 1973). These methods provide useful indirect data in thickness studies when combined with dimensional characteristics of craters. Remote geochemical sensing techniques are able to differentiate terra or upland materials from mare basalts. Where sufficient resolution exists, it is possible to recognize the signature of terra material in the rims of craters within mare basalts. Two possible uses of the data are suggested:

1. For pre-mare craters - Detection of terra materials in the exposed rim of partially buried craters would verify that the craters formed on a pre-basalt surface and would yield proper values for the thickness of the basalts. Partially buried craters with only mare materials in the rim would be excluded from the thickness data, as

these craters have formed within the mare basalt sequence.

2. For post-mare craters - Any crater yielding a terra signature would indicate that the crater penetrates the mare basalts. The depth of the crater floor below surface level for the smallest crater to yield terra material would be an indication of basalt thickness.

Unfortunately, the present limitations of resolution will not allow detection of the small areas involved in crater rims nor of small craters.

BASIN DESCRIPTIONS

Mare Serenitatis

Mare Serenitatis is a well defined, 700 km diameter, multiringed basin with a prominent mascon (Muller and Sjogren, 1968). The basin is probably the site of two or more overlapping impact basins (Scott, 1974; Maxwell et al., 1975). The mare surface averages 4500 m elevation in the southern half of the basin with a well developed trough which is less than 4500 m elevation in the eastern portion of the mare.

The mare ridge and arch pattern of Mare Serenitatis is described by Howard and Muehlberger, (1973) and by Maxwell et al., (1975). In the southern half of the basin, the ridge pattern can be described as three nested rings which overlap or coincide in the south (Fig. 7). The largest ring (750 km diameter) is defined by arcuate ridges parallel and close to the mare/terra contact. The next ring (350 km. diameter) forms an almost complete circle marking mid-basin. The third ring (200 km diameter) is centered on the southeastern mare surface. The eastern trough lies between the outer ring and the coincident second and third rings. Prominent families of rilles are located along the southwestern, southern, and southeastern borders of the basin (Fig. 7). As in most basins, the

rilles occur parallel to sub-parallel to the basin edge. In the southeastern region near Littrow the rilles are traced into the surrounding terra.

The isopach map and the map of the basin floor are based on only six data points in southeastern Serenitatis (Fig. 8). The results are necessarily problematical and indicative. Nevertheless, the development of a trough in the southeastern part of the basin is apparently real. The trough is probably low lying terrain between the buried inner raised ring and the next outward ring. The lack of buried craters within this region suggest that this rimmed shelf is buried by moderate to thick mare basalts. The central part of the basin is not measured, but estimates of 3.5 km depth (Hartman and Wood, 1971) are not unreasonable.

Mare Tranquillitatis

Mare Tranquillitatis occupies an extensive shallow mare basin near the lunar equator (Fig. 5 and 9). The surface is approximately 750 km by 525 km and covers an area of 430,000 km². The basin has been variously classified as a degraded multiringed impact basin (Wilhelms and McCauley, 1971; Head, 1975); a multiple impact basin (Stuart-Alexander and Howard, 1971); and a shallow, irregular basin (DeHon, 1974). Sinus Amoris is

a 200 km long embayment extending northward from north east Mare Tranquillitatis.

The contact of mare and terra materials in the Tranquillitatis basin is 6000 m in the west and 6200-6500 m in the east. The mare surface slopes gently to a minimum elevation along a north-south line through the midwestern portion of the basin (Fig. 4). The lowest elevation (less than 5000 m) is reached in the area of the circular feature Lamont. Sinus Amoris exhibits a northward slope from 6200 m in the south to 5200-5400 m in the north.

Surface features at Mare Tranquillitatis (Fig. 9) include rilles, mare ridges, and mare domes. Prominent arcuate rilles occur in northern Tranquillitatis in the opening between Mare Tranquillitatis and Mare Fecunditatis; as sets or families of rilles parallel to the western and southwestern edge of the basin; and as a set of rilles and scarps in northeastern Tranquillitatis. Mare ridges form a conspicuous circular and radial pattern in the southwestern part of the basin. The innermost ring of ridges defines the feature Lamont. Low domes, circular to irregular in plan view, are found on the northeastern portion of the basin; in an aligned series north of the crater Arago; and as scattered domes in the southeastern part of the basin.

The thickness of mare basalts in the Tranquillitatis

and Sinus Amoris basins (Fig. 10) averages 500 m thick. The thickest basalts in Sinus Amoris are slightly over 750 m thick in the southern end of the embayment. Basalt thicknesses in excess of 750 m in the Tranquillitatis basin occur in a large mid-basin area and in smaller peripheral lenses to the north and east. The thickest basalts (greater than 1250 m) are located in the region of Lamont.

A map of the basin floor (Fig. 6) gives a generalized picture of the basin configuration beneath the basalt fill. In general, the basin floor maintains the trends observed in the surface topography. Sinus Amoris occupies a well-defined trough which slopes northward, and a shallow rill separates the two basins. The floor of Tranquillitatis reaches its lowest elevation southeast of Lamont.

The Tranquillitatis basin structure is probably a composite of several overlapping and superposed structural trends. The depression in the region of Lamont may represent the remnants of a multiringed impact basin, but if it is an impact basin, it has been highly degraded. Any other impact basins within the Tranquillitatis region as suggested by Head (1975) or Stuart-Alexander and Howard (1971) are similarly degraded to near unrecognizable form. The tranquillitatis region is crossed by several structures peripheral to

younger circular basins. The northern portion of Tranquillitatis is within a circum-Serenitatis belt of low lying terrain which includes Sinus Amoris. The southern part of the basin includes a circum-Nectaris trough, and the southeastern part of the basin is included in a possible trough concentric to the central Fecunditatis basin.

Mare Nectaris

Mare Nectaris is a 350 km diameter mascon multi-ringed basin (Wilhelms and McCauley, 1971; Hartmann and Woods, 1971). The mare surface extends northward through a 150 km wide trough to connect with Mare Tranquillitatis (Fig. 5 and 11). A broad positive gravity anomaly occurs over the trough in the vicinity of the crater Torricelli (Sjogren et al., 1974; Scott, 1974).

Surface elevations are known only for the Apollo 16 photographic strip (Fig. 12a) which crosses the trough between Mare Nectaris and Mare Tranquillitatis. The mare surface in this region slopes from an average 5500-6000 m elevation to a broad depression less than 5000 m in the region of Torricelli. The northernmost surface of Nectaris slopes downward toward the center of the basin.

Surface features are sparse (Fig. 11). A north-south trending series of ridges extends from southern Tranquillitatis into the central part of the trough where the trend changes to coincide with the northern rim of the buried crater Torricelli R. A few scattered ridges occur around the edges of the Nectaris disk. One arcuate rille parallels the northeastern edge of the basin, and a few scattered domes are identified in the northern part of the basin.

The isopach and basin floor maps (Fig. 12b and 13) are constructed from data points occurring within the trough and in the northern part of the Nectaris basin. Ejecta from the large Copernican-aged crater Theophilus masks a large portion of surface, and as in all deep circular maria the thicker interior cannot be measured by buried craters. Hence, the thickening trend observed at the edges of the basin have been projected toward the area of maximum gravity anomaly. A projected thickness of 3000-4000 m is indicated, but the actual thickness is dependent on the real slopes and mid-basin configuration. The thickening trend of mare basalts in the basin suggests that the basalts do not flood a shelf as observed in most other circular basins (Wilhelms and McCauley, 1971; DeHon, 1974). Within the trough to the north the thickness is measured in excess of 1000 m along much of its

length, and a maximum in excess of 1250 m occurs in the region of Torricelli R coincident with the gravity high in the region. Scott (1974) derives a thickness of 1800 m in the region by gravity modeling.

Mare Crisium

Mare Crisium (Figs. 5 and 14) is a 475 km diameter multiringed basin (Olson and Wilhelms, 1974). The mare basalts occupy the deep central basin and flood a shelf of variable width. Flooding extends beyond the most prominent raised ring to the east to give the basin an overall elliptical outline (Wilhelms, 1973). A well defined mascon occurs in the western part of the basin (Sjogren, 1974).

Topographic coverage is available for the southern half of the mare (Fig. 15). The mare surface is approximately 3750-4000 m along the basin edge, and it is terraced downward toward the interior. The interior of the basin is relatively level at 3250 m elevation. Prominent mare ridge trends form a circumferential pattern near the basin edge and two interior patterns which traverse mid-basin (Fig. 14).

As in other circular maria, partially buried craters are limited to the shallow shelf areas. The isopach and basin floor maps (Fig. 15b and 16) are based on a

a small number of exposed craters on the southern shelf. The data project an increasing thickness of basalt to the southwestern portion of the basin north of the crater Picard in the vicinity of the high gravity anomaly.

The basin related structures in the Crisium region are more or less typical of all multiringed basins. Four raised rings are delineated (Wilhelms, 1973) approximately 210, 250, 340, and 485 km from the basin center. The sparse thickness data suggest that the flooded portion of the basin is similar to that of the Serenitatis basin. A deep inner basin is probably outlined by the mare ridge pattern roughly 210 km in diameter centered at 17°N ; 56°E . A deep crescent shaped shelf probably exist between 60° and 65°E (Fig. 15). The overall elliptical outline of the basin is caused by the flooding of basalts over the second raised rim into the peripheral low lying terrain to the east.

Mare Fecunditatis

Mare Fecunditatis is an irregularly shaped basin 600 km by 900 km across (Fig. 15 and 17). In the north mare deposits may occupy a circular basin (Stuart-Alexander and Howard, 1970; Hartmann and Wood, 1971; Wilhelms and McCauley, 1971) or a highly degraded circular basin (Head, 1975; DeHon, 1975b). Mare materials

in the south flood low lying cratered terrain. A weak gravity anomaly is centered on the northern part of the basin (Sjogren, 1974).

The mare surface slopes from about 6000 m elevation in the west to 5250 m along the eastern margin (Fig. 18). A broad trough trends northwesterly in the northeastern portion of the mare surface, and the mare surface is terraced downward to a broad low area (less than 5250 m elevation) near the center of the basin.

The mare ridge pattern is analyzed by Waskom and DeHon (in prep.). The most prominent trends are associated with the family of ridges which trend north-northeast through the central mare and form an arc around the western and northern edges of the central mare low. (Fig.17). Other ridges are radial to the central mare depression or nearly parallel to the basin edge. Rilles display two prominent patterns. Most rilles are parallel to the basin edge, but a few project into the mare perpendicular to the mare shoreline.

The isopach map (Fig. 19) reveals local thickening of mare basalts in excess of 500 m at the northern end of the basin; within a small eastern embayment; and in a large area of the western and central part of the basin. A basalt thickness in excess of 1000 m in the central

basin is modeled by using the arc of the ridge trend in this region as the diameter of buried crater. The reconstructed basin floor (Fig. 20) is characterized by broad depressions which are located in the same positions as surface depressions. Data in southern Fecunditatis are insufficient to complete an isopach map with certainty, but the region is probably shallow.

The present configuration of the Fecunditatis basin is probably a composite of overlapping structures (Waskom and DeHon, in prep.). The central deep portion may be a localized depression or an extensively modified multi-ringed basin (DeHon, 1975b). The northeastern portion of the basin lies on an arc of lowlying terrain concentric to Mare Crisium which includes Mare Undarum, Mare Spumans, and mare basalts near the crater Macrobius. The western half of the basin lies on an arc concentric to Mare Nectaris which includes southern Tranquillitatis and low lying terrain beyond the Atlas scarp.

Mare Spumans and Mare Undarum

Mare Spumans and Mare Undarum are small irregular patches of mare material southeast of Mare Crisium and east of northern Mare Fecunditatis (Fig. 5). The basins are located along the axis of a trough concentric to Mare Crisium (DeHon, 1975a). The mare surface covers

approximately 55,000 km². The regional topography consist of a broad irregular trough trending northeast-southwest sloping toward Mare Fecunditatis to the southwest (Fig. 21). The smoothness of the mare surface is broken by many isolated massifs of highland terrain which project through the mare lavas and irregular benches of mare material standing at different levels. Rilles and mare ridges are absent.

Three crater populations in the Spumans and Undarum region are recognized by DeHon (1975a). The oldest craters, older than the Crisium basin, are degraded and partially filled by Crisium ejecta; hence, they cannot be used in thickness estimates. Craters formed after the emplacement of Crisium ejecta blanket and prior to flooding by mare basalts are used to estimate basalt thicknesses. Craters superimposed on the mare surface cannot be used to estimate basalt thickness. An average of 200 m of basalt is obtained throughout the basins with a 900 m maximum in the southern end of the materials (Fig. 22). - Local lenses in excess of 600 m are scattered throughout the basins. - Most local lensing reflect the influence of the older, degraded craters flooded by mare basalts. The reconstructed basin floor (Fig. 23) -- maintains the trough-like configuration observed in the surface topography which is attributed to the formation

of a circum-mare trough between the third and fourth raised rings of the Crisium basin (DeHon, 1975a).

Mare Smythii

The Smythii basin is a degraded circular basin 370 km in diameter (Stuart-Alexander and Howard, 1970; Stewart, Waskom and DeHon, 1975; Brennan, 1975). Mare material is limited to an area approximately 200 km diameter (Fig. 24) and isolated lenses within some of the larger craters. The mare deposits is classed as an incipient basin fill (Type IB2 of Head, 1975). A well defined mascon is centered over the mare basalt lens (Sjogren, 1974).

The floor of the Smythii basin consists of smooth plains and mare material in the northern part of the basin and a more cratered and hummocky material of a crescent-shaped shelf occupies the western and southern two-thirds of the basin (Fig. 24). The hummocky material is generally level at the 500 m contour interval with a regional slope toward the mare materials. The surface of the mare basalts is smooth with a few mare ridges along the northern and eastern edges of the basin. The lowest elevation on the floor of the basin (less than 3500 m) occurs within the mare basalts (Fig. 25a).

An isopach map (Fig. 25b) of the combined-floor materials (Stewart, Waskom, and DeHon, 1975) indicates a

a probable thickness of materials averaging 500 m with local lensing in excess of 750 m. The mare basalts, however, reach a total thickness of only 500-600 m in the northern floor of the basin. The reconstructed basin floor (Fig. 25c) shows the mare basalts filling a shallow eccentric inner basin on the floor of the Smythii basin. Isolated patches of basalt occur within large craters formed on the crescent shelf that floors the basin.

CORRELATIONS

Surface Topography

The basalt surface of the lunar maria is lower than the surrounding terra by several hundreds of meters. Within the maria there is a close correlation between the local mare surface elevation and the thickness of basalt. The mare surface is invariably depressed in the region of thick basalts (Table I). In the circular maria (such as Mare Serenitatis, Mare Nectaris, and Mare Crisium) the surface is terraced or slopes down to the area of maximum positive gravity anomaly which is assumed to be the zone of maximum thickness. In the shallow irregular basins, local depressions of the mare surface coincide with lenses of thickest basalt (such as the region of Lamont in Mare Tranquillitatis, Torricelli, and the multiple lenses in Mare Fecunditatis).

The correlation between surface elevation and basalt thickness could arise from either isostatic sinking in response to the load placed on the surface by the mare basalts or from volume reduction of the basalts during cooling and consolidation. Distinguishing between these two factors is important in defining the internal strength of the moon and reconstruction of the pre-basalt topography. If the moon is capable of isostatic

deformation in response to the relatively thin basalts, then the reconstructed basin floor reflects this modification. If, to the contrary, the moon's surface is rigid, then the reconstructed basin floor reflects paleotopography existing prior to emplacement of the mare basalts.

Further, this observation emphasizes the fact that the geometry of the mare surface provides insight into the relative thickness of mare basalts and corresponding configuration of the basin floor. Regional topographic maps (based on stereophotography, laser altimetry, or radar methods) can provide guides to sub-basin structure.

Mascon and Basalt Thickness

Gravity measurements derived from Lunar Orbiter spacecraft accelerations resolved positive gravity anomalies associated with the major multiringed basins (Muller and Sjogren, 1968). Subsequent measurements from Apollo orbits provide improved resolution and reveal smaller mascons within irregular and degraded mare basins (Sjogren et al., 1972; Sjogren et al., 1974). Models of the mascons have included deeply buried spherical iron meteorites (Stripe, 1968; Urey, 1968); thin surface disks (Conel and Holstrom, 1968; Baldwin, 1968; Wood, 1970), and relief on the lunar mantle (Wise

and Yeats, 1970). A composite structure of mantle plug and surface disk is suggested by Phillips et al., (1972), Head (1975) and Sean (1975).

Mascons are associated with areas of increased basalt thickness (Table II) within both multiringed basins and irregular maria. Positive gravity anomalies of the major multiringed basins match the central basin as defined by the mare ridge pattern (Phillips, et al., 1972). Smaller "mini-mascons" are associated with local thick lenses within irregular and degraded basins (Sjogren, 1975). In general, positive gravity anomalies occur over areas where basalt thickness exceeds 1000 m. One striking exception to the rule is the gravity high associated with the Mare Smythii basalts which are less than 750 m thick. The thin basalts and positive anomaly in the Nectaris basin (Head, 1975) and the similar occurrence in Smythii (DeHon, 1975b; Stewart, Waskom, and DeHon, 1975) would tend to support a combination of mantle plug and surface disk origin for at least some mascons.

The basalt lenses at Lamont, Torricelli R, and central Fecunditatis are modeled on the assumption that mare ridge-rings represent the diameter of a buried crater, and that the average basalt thickness in the region is represented by the calculated rim height of

the buried crater. The interior depth of the crater or possible deformation from a fresh crater form is not considered. The thickness shown in the isopach map, therefore, provides a generalized construction for gravity modeling, but absolute thickness may be greater than that shown.

Mare Ridges---

Mare ridges are prominent surface features of almost all larger maria, but they are sparse or lacking in the smaller irregular and thin patches of maria material. The general distribution of ridges within mare basins has been depicted by (Baldwin, 1949 and 1963; Hackman and Mason, 1961; Scott et al., 1975). A multitude of hypotheses have been used to explain the origin of mare ridges. These include 1) draped subjacent topography (Baldwin, 1963; Maxwell et al., 1975); 2) intrusive or extrusive volcanism including autoinstursion (Whitaker, 1966; Strom, 1972; Hodges, 1973; Scott et al., 1975) 3) tectonic deformation resulting from shrinkage and isostatic subsidence of mare lava flows (Bryan, 1973); 4) tectonic formation due to crustal compression accompanied by thrusting (Schaber, 1973; Howard and Muehlberger, 1973; Muehlberger, 1974). A combination of processes are favored by Tjial (1970); Hartmann and

Wood (1971), Colton et al. (1972).

Four patterns of mare ridge distribution are apparent in regional distributions (Fig. 26). Basin concentric systems are associated with the major circular mare basins and mark the outer ridge of the gravity high. Interbasinal concentric and radial patterns are usually found associated with small, local gravity highs. Roughly linear or arcuate ridge patterns occur in mid-basin of some maria. Finally, small arcs and circles of ridges are observed marking the buried edges of partially buried craters or the entire rim crest of completely buried craters. The outer ring of ridges in Mare Serenitatis, Mare Nectaris, and Mare Crisium serve as examples of the large basin concentric patterns. Radial patterns are best developed in Mare Tranquillitatis. Transverse ridge patterns are present in mid-Serenitatis, mid-Crisium, and Mare Fecunditatis. Smaller arcs and circles associated with buried craters are prominent in most basins.

Mare ridge patterns follow a close correlation with other-features of the maria. The basin concentric ridge systems correspond to the edges of the mascon within a major circular mare such as Serenitatis (Phillips et al.; 1972; Maxwell et al.; 1975), Crisium, and Nectaris. Interbasinal concentric ridge patterns mark

the location of small gravity highs at Lamont, Toricelli R, and central Mare Fecunditatis. Within concentric ridge patterns the mare surface is normally depressed. Some ridges mark the edges of a downward terraced mare surface. Locally, ridges develop nearly monoclinial structure with the lower side toward the basin interior.

When ridge patterns are compared with the isopach map (Fig. 5) or the basin floor map (Fig. 6) a close correlation is found between changes in basalt thickness and ridge location. Mare ridges are localized in areas of increasing basalt thickness or significant changes in the slope of the basin floor. Ridges are not found in regions of uniformly thin basalt nor are they found on the surface over uniformly thick basalts.

Mare ridges are largely surface compressional features localized by the configuration of the basin floor. As the mare lavas undergo volume reduction upon consolidation, the surface sags, developing tension at the edges, but away from the edges the surface is subjected to compressional stress. The slope of the basin floor tends to localize the compressive stress; hence, buckling of the surface occurs. Similar effects are noted in Hawaiian lava crust which bury pre-existing craters (Cruikshank *et al.*, 1973). Draping of lavas over local positive basement relief is also part of the process, inasmuch as most of the changes in slope are also

sites of crater rims or buried basin rims. The disruption of the basin floor slopes would also tend to localize autointrusion (Hodges, 1973). Thus, while ridges are compressive surface features, they may also be the site of other processes including autointrusion, thrusting or extrusion.

Mare Domes

Mare domes are smooth low features with gentle convex upward profiles. They are circular to elliptical and are generally less than 15 km in diameter. Small summit craters may or may not be present. Isolated domes may be found in almost all maria, but significant concentrations occur in the Stadius region and in Mare Tranquillitatis.

The domes are commonly interpreted as shield volcanoes (Pickering, 1908; Wilhelms and McCauley, 1971) or laccoliths (Marshall, 1943; Spur, 1945; Baldwin, 1963, Wilhelms and McCauley, 1971). Head (1975) has proposed that the domes might be more analogous to basalt plains domes as described by MacDonald (1972).

The location of domes (Fig. 26) compared to basalt thickness (Fig. 5) or basin floor topography (Fig. 6) exhibits a wider range of scatter than other surface features. Two domes in Mare Crisium appear to be associated with the transverse ridge system. Two domes

in Mare Nectaris occur along the edge of the basalts in the region of mare ridges and one dome is found over the deeper interior of the mare basalts. Mare Tranquillitatis contains the most prominent collection of domes of the eastern maria (Fig. 9 and Fig. 26). Domes occur on the northeastern surface, east of Jansen and on the west central surface, north of Arago. The domes of the western surface form a chain radial to Lamont and are localized along the northwest thickening zone of basalts. The domes of the eastern surface display three associations: 1) on the thinner basalts over the sill between Mare Tranquillitatis and Sinus Amoris; 2) irregular scatter around the thick basalt lens east of Jansen; and 3) over moderately thick basalts (500-750 m thick) southeast of Jansen parallel to the Cauchy rille trend.

Mare domes are not shield volcanoes in the classic sense as they lack many of the features common to shields (Head, 1975; Baldwin, 1963). The domes may be laccolith-like structures or basalt plains domes. They may not be of deep crustal origin, but rather intrusions or extrusions escaping from local lava pockets along zones of deformed or fractured mare basalts.

Arcuate Mare Rilles

Graben-like arcuate mare rilles are common features in all but the smallest mare basins. The distribution of rilles has been mapped by numerous investigators including Baldwin (1949, 1963), Hackman and Mason (1961), and Scott et al. (1975). They form gently curving or arcuate patterns often in enechelon series parallel or sub-parallel to basin edge (Fig. 26). Most arcuate rilles are confined to the mare basalts, but a few are continuous into the nearby terra. There is a concensus of opinion that the rilles are fault graben developed in response to tension in the mare basalts at the edges of the basins (Baldwin, 1963; Quaide, 1966; Smith, 1966; McGill, 1971). Similar tensional zones are common in the subsidence surface over buried volcanic craters (Swanson and Peterson, 1972).

All rilles are restricted to thin mare basalts (less than 500 m thick) and are parallel or sub-parallel to zones of equal thickness. The data is consistent with a model of rilles of shallow tensional stress origin in which the stress is decoupled or loosely coupled with the underlying basement. The shallow stress field probably results from basalt consolidation and volume reduction or settling. Those rilles which are continuous into the surrounding terra are probably localized along fractures existing before mare-filling.

IMPLICATIONS

Estimates of volumes of basalts erupted during the mare filling stage of lunar history are based on estimates of average basalt thickness ranging in excess of 20 km (Toksoz, 1973); to 1000-2000 meters (Moore et al., 1974). The total volume of basalt in the mare basins is relatively small based on the thicknesses derived in this study (Table III), and may be less than one percent of the total crustal volume (Head, 1975). The relatively thin layer of basalts provides important limits to various modes of lunar crustal structure and past lunar processes.

As the total volume of mare basalt is reduced so also is internal heat needed to generate the basalts by partial melting within the moon. The somewhat complex restraint of a late period (late Imbrian) of high heat flux is reduced. The magma source regions represent an extremely small portion of the total volume of the zone capable of melting and melting was not wide spread (Head, 1975).

Isostasy, which may have been an important process in early lunar history, was not a major operational internal process by mid-Imbrian time. The large gravity anomalies are, in part, explained by mantle plugs. (Wise and Yeats, 1969) and, in part, by superisostatic loads

of mare basalts on the lunar crust. Isostatic compensation may have played a more important role in early lunar history. The mechanisms by which originally deep circular basins are degraded include multiple impact, infilling by throwout from other large basins, volcanic flooding and isostasy. Young basins such as Orientalis, Imbrium, and Serenitatis contain well developed mascons. Old basins such as Mare Nubrium do not contain extensive mascons. The deeper interiors of Mare Tranquillitatis and Mare Fecunditatis do not have the form or gravity anomaly of younger multiringed basins. If these basins originated in the same manner as the younger basins, they may have lost much of the multiring characteristics by isostatic compensation.

The general form of the multiring circular basins is agreed upon by most lunar investigators (Baldwin, 1949; Hartmann and Kuiper, 1962; Shoemaker and Hackman, 1962; Stuart-Alexander and Howard, 1970). The analysis of partially buried craters provide a slight refinement of the structure of circular basins in the region of the shallow shelf. Within the central part of the basins the basalts are too thick to reveal any craters on the basin floor. The correlations of mare ridges with floor structure does provide some insight into the inner basin structure (DeHon, 1975b; Waskom and DeHon,

1975 ; Maxwell et al., 1975). The structure of shallow maria is revealed by analysis of partially buried craters. Relatively deep sub-basins and troughing trends are detected as well as broad rises of the basin floors. Much of the intra-basinal structure can be related to circum-mare structures formed in response to younger, multiringed mascon basins (DeHon, 1974, 1975a; Waskom and DeHon, 1975).

The relative thinness of mare basalts has important implications for lunar gravity anomalies. Young deep basins with thick mare basalts have well defined mascons. Shallow maria with thin basalts exhibit little positive gravity anomaly. Moderately deep fill in Lamont and mid-Fecunditatis, exhibit small anomalies. Relatively thin basalts in Mare Smythii are associated with a positive mascon. It seems unlikely that the thin disk of mare materials in Mare Smythii can account for the mascon. It is probable that the mascon in all basins is produced by two components; a mantle plug and surface disk of basalts.

The isopach maps, basin-floor maps, and their correlations with surface features provide some implications to the mode of emplacement of mare basalts. Most surface features can be explained in terms of modification of the basalt surface by primarily passive forces asso-

iated with the emplacement of basalts on a rigid surface. Surface features of the basalts formed in response to stresses developed within the basalts and not external to the basalts. The basins filled as a consequence of their low elevation from source vents covered by their own effluent. The sources cannot be uniquely identified; however, the basin floor topography provides some insight into limitations. Some, if not all, basalts were extruded along fractures related to the multiringed basins. Filling of the flooded craters and basins is primarily hydrostatic (Scott et al., 1975). Mare basalts were apparently emplaced in a manner similar to terrestrial plateau flood basalts (Greely, 1975). Therefore, the lunar maria can be expected to yield similar histories, structures, reservoirs and rates of production at plateau basalts rather than features common to shield-type basalts.

ACKNOWLEDGEMENTS

This work was performed as NASA Experiment S-221 at the University of Arkansas at Monticello under Contract No. NAS 9-13196. The help of Mr. James Fletcher, Mr. Charles Gunn, and Mrs. Nell Cooley is gratefully acknowledged.

REFERENCES

- Adler, I., Trombka, J., Lowman, P., Schmadebeck, R., Glodget, H., Eller, E., Yin, L., Lamothe, R., Oswald, G., Gorgenstein, P., Bjorkolm, P., Gursky, H., Golub, L., and Harnden, F. R., (1973) X-ray fluorescence experiment: Apollo Preliminary Sci. Report, NASA SP 315, 19-1--19-14.
- Baldwin, R. B. (1949) The face of the moon: University of Chicago Press, Chicago, Ill. 239.
- Baldwin, R. B. (1963) The measure of the moon: University of Chicago Press, Chicago, Ill. 488.
- Baldwin, R. B. (1968) Lunar mascons: Another interpretation: Science, 162, 1407-1408.
- Baldwin, R. B. (1970) A new method of determining the depth of the lava in lunar maria: Publ. of the Astron. Soc. of the Pacific., 82, 857-864.
- Brennan, W. J. (1975) Evolution of Mare Smythii: in Lunar Science VI, Lunar Science Institute, Houston, Tex., 86-88.
- Bryan, W. B. (1973) Wrinkle-ridges as deformed surface crust on ponded mare lava: Geochim. Cosmochim. ACTA, 37, suppl. 4, 93-106.
- Colton, G. W., Howard, K. A., and Moore, H. J. (1972) Mare ridges and arches in southern Oceanus Procellarum: Apollo 16 Preliminary Science Report, NASA Spec. Publ. SP-315, 29-90--29-93.
- Conel, J. E., and Holstrom, G. B. (1968) Lunar mascons: A near surface interpretation: Science, 162, 1403-1404.
- Cruikshank, D. P., Hartmann, W. K., and Wood, C.A. (1973) Moon: 'Ghost' craters formed during mare filling: Moon, 7, 440-452.
- DeHon, R. A. (1974) Thickness of mare material in the Tranquillitatis and Nectaris basins: Geochim. Cosmochim. ACTA, 38, suppl. 5, 53-59.

**ORIGINAL PAGE IS
OF POOR QUALITY**

- DeHon, R. A. (1975a) Mare Spumans and Mare Undarum: Mare thickness and basin floor: Proc. Lunar Sci. Conf. 6th. in press.
- DeHon, R. A. (1975b) An isopach map of the eastern mare basalts: in origins of mare basalts and their implications for Lunar Evolution : Lunar Sci. Institute, 29-31.
- DeSitter, L. U. (1956) Structural Geology, New York: McGraw-Hill, 551.
- Eggleton, R. E. (1963) Thickness of the Apenninian series in the Lansberg region of the moon: Astrogeologic Studies Annual Progress Report, Aug. 25, 1961 to Aug. 24, 1962. U. S. Geo. Survey open-file Report, 19-31.
- Eggleton, R. E., Schaber, G. G. and Pike, R. J. (1974) Photogeologic detection of surfaces buried by mare basalts: Lunar Science: The Lunar Science Institute, Houston, 200-202.
- Greeley, R. A. (1975) A model for the emplacement of lunar basin-filling basalts: Lunar Science VI, Lunar Sci. Inst. Houston, Tex., 309-310.
- Hackman, R. J., and Mason, A. C. (1961) Engineer special study of the surface of the moon: U. S. Geol. Surv. Misc. Inves. Map I-351.
- Hartmann, W. K. and Kuiper, G. P. (1962) Concentric structures surrounding lunar basins: Commun. Lunar Planetary Lab. 1, 51-67.
- Hartmann, W. K., and Wood, C. A. (1971) Moon: Origin and evolution of multiring basins: Moon, 3, 3-78.
- Head, J. W. (1975a) Processes of lunar crater degradation changes in style with time: Moon (in press).
- Head, J. W. (1975b) Lunar volcanism in space and time: Reviews of Geophys. and Space Phys., (in press).
- Hodges, C. A. (1973) Mare ridges and lava lakes: Apollo 17 Preliminary Science Report, NASA Spec. Publ. SP-330, 31-12--31-21.

- Howard, K. A. (1970) Mascons, mare rock, and isostasy: Nature, 226, 924-925.
- Howard, K. A., and Muehlberger, W. R. (1973) Lunar thrust faults in the Taurus-Littrow region: Apollo 17 Preliminary Science Report, NASA Spec. Publ. SP-330, 29-1.
- Kaula, W. M. (1969) Interpretation of lunar mass concentrations: Phys. Earth Planet. Interiors, 2, 123-137.
- Kovach, R. L., Watkins, J. S., and Talwon, P. (1973) Lunar seismic profiling experiment: Apollo 17 Preliminary Science Report, NASA Spec. Publ. SP-330, 10-1--10-12.
- Latham, G., Ewing, M., Press, F., Sutton, G., Dorman, J., Hakamura, Y., Toksoz, N., Wiggins, R., Derr, J., and Duennebier, F. (1970) Apollo 11 passive seismic experiment: Science 167, 455-467.
- MacDonald, G. A. (1972) Volcanoes: Prentice-Hall, Englewood Cliffs, N. J.
- Marshall, C. H. (1963) Thickness and structure of the Procellarian system in the Lansberg region of the moon: Astrogeologic studies annual progress report, Aug. 25, 1961 to Aug. 24, 1962. U. S. Geol. Survey Open-File Report, 19-31.
- Marshall, R. K. (1943) The origin of lunar craters: Pop. Astr. 51, 415.
- Maxwell, T. A., El-Baz, Farouk, and Ward, S.H. (1975) Distribution, morphology and origin of ridges and arches in Mare Serenitatis: Geol. Soc. Amer. Bull., 86, 1273-1278.
- McCord, T. B., Charette, M. P., Johnson, T. V., Lebofsky, L. A. and Pieters, C. (1972) Spectrophotometry (0.3 to 1.1 micron) of proposed Apollo lunar landing sites: Moon, 5, 52-89.

ORIGINAL PAGE IS
OF POOR QUALITY

- McGetchin, T. R., Settle, M., and Choet, B.A. (1974) Cinder cone growth modeled after Northeast crater, Mt. Etna, Sicily: J. Geophys. Res., 79, 3257-3272.
- McGill, G. E. (1970) Attitudes of fractures bounding straight and arcuate rilles: Icarus 14, 53-58.
- Moore, H. J. Hodges, C. A., and Scott, D. H. (1974) Multiringed basins illustrated by Orientale and associated features: Geochim. Cosmochim. ACTA, 38 Suppl. 5, 71-100.
- Muehlberger, W. R. (1974) Structural history of southeastern Mare Serenitatis and adjacent highlands: Geochim. Cosmochim. ACTA, 38, Suppl. 5, 101-110.
- Muller, P. M., and Sjogren, W. L. (1968) Mascons: Lunar mass concentrations: Science 161, 680-684.
- Olson, A. B., and Wilhelms, D. E. (1974) Geologic map of the Undarum quadrangle of the moon: U. S. Geol. Surv. Misc. Geol. Inv. Map I-837.
- Phillips, R. J., Adams, G. F., Brown, W. E., Jr., Eggleton, R. E., Jackson, P., Jordan, R., Linlor, W. I., Peeples, W. J., Porcello, L. J., Ryu, J., Schaber, G., Sill, W. R., Thompson, T. W., Ward, S. H., and Zwilensky, J. S. (1973) Apollo Lunar sounder experiments: Apollo 17 Preliminary Science Report, NASA Spec. Publ. SP-330, 22-1--22-26.
- Phillips, R. J., Conel, J. E., Abbott, E. A., Sjogren, W. L., and Morton, J. B. (1972) Mascons: Progress toward a unique solution for mass distribution: J. Geophys. Res., 77, 7106-7117.
- Pickering, W. H. (1908) L'origine de la lune et la probleme des volcans: Soc. Belge Astron, Bull., 13, 71-74.
- Pieters, C., Head, J. W., McCord, T.B., Adams, J. B., and Zisk, S. (1975) Geochemical and geologic units of Mare Humorum; definition using remote sensing and lunar sample information: Proc. Lunar Sci. Conf. 6th, (in press).

- Smith, G. K. (1966) A comparison of two terrestrial graben with the lunar rilles Rima Ariadaeus and rimae Hypatia I and II. U. S. Geol. Surv. Astrogeol. Studies, ptA, 65-86.
- Spurr, J. E. (1945) Geology applied to selenology: The features of the moon, Science Press, Lancaster, Pa., 430.
- Stewart, H. E., Waskom, J. D., and DeHon, R. A. (1975) The photogeology and basin configuration of Mare Smythii: Proc. Lunar Sci. Conf. 6th, (in press).
- Stipe, J. G. (1968) Iron meteorites as mascons: Science, 162, 1402-1403.
- Strom, R. G. (1972) Lunar mare ridges, rings and volcanic ring complexes: Modern Geol., 2, 133-157.
- Stuart-Alexander, D. E. and Howard, K. A. (1971) Lunar maria and circular basins - A review: Icarus, 12, 440-456.
- Swanson, D. A. and Peterson, D. W. (1972) Partial draining and crustal subsidence of Alae lava lake: U. S. Geol. Survey Prof. Paper 800 C, 14.
- Tjia, H. D. (1970) Lunar wrinkle ridges indicative of strike-slip faulting: Geol. Soc. Amer. Bull. 81, 3095-3100.
- Toksoz, M. N., and Solomon, S. C. (1973) Thermal history and evolution of the moon: Moon, 7, 251-278.
- Urey, H. C. (1968) Mascons and the history of the moon: Science 162, 1408-1410.
- Waskom, J. D. and DeHon, R. A. (1976) Mare Fecunditatis: mare ridges and basin structure, (in prep).
- Whitaker, E. A. (1966) The surface of the moon: in the nature of the lunar surface: Proceedings of the 1965 IAU-NASA Symposium, edited by W. N. Hess, D. H. Menzel, and J. A. O'Keefe, John Hopkins, Baltimore, Md., 79-98.

- Pike, R. J. (1967) Schroeter's rule and the modification of lunar impact morphology: J. Geophys. Res. 72, 2099-2106.
- Pike, R. J. (1972) Geometric similitude of lunar and terrestrial craters: Proc. of the 24th Internat'l Geol. Cong. (Montreal), Sec. 15, 41-47.
- Pike, R. J. (1974) Depth/diameter relations of fresh lunar craters--Revision from spacecraft data: Geophys. Res. Letters, 1, 291-294.
- Quiade, W. L. (1965) Rilles ridges and domes - clue to maria history: Icarus, 4, 374-389.
- Schaber, G. G. (1973) Lava flows in Mare Imbrium: geologic evaluation from Apollo orbital photography: Proc. of Lunar Sci. Conf. 4th, 73-72.
- Scott, D. H. (1974) The geologic significance of some lunar gravity anomalies: Geochim. Cosmochim. ACTA, 38, suppl. 5, 3025-3036.
- Scott, D. H., Diaz, J. M., and Watkin, J. A. (1975) The geologic evaluation and regional synthesis of metric and panoramic photographs: Proc. Lunar Sci. Conf. 6th, (in press).
- Settle, M. and Head, J. W. (1975) Topographic variations in lunar crater rim profiles - implications for the formation of ejecta deposits: Icarus, (in press).
- Shoemaker, E. M., and Hackman, R. J. (1962) Stratigraphic basis for a lunar time scale: Moon (Z. Kopal, ed.): Academic Press, New York, 289-300.
- Sjogren, W. L. (1974) Lunar gravity at 100 km altitude: Proc. Lunar Sci. Conf. 5th, 1, Plate 1.
- Sjogren, W. L., Gottlieb, P., Miller, P. M., Wollenhaupt, W. (1972) Lunar gravity via Apollo 14 doppler radio tracking: Science 175, 165-168.
- Sjogren, W. L., Wollenhaupt, W. R., and Wimberly, R. N., (1974) Lunar gravity via the Apollo 15 and 16 subsatellite: Moon, 9, 115-129.

ORIGINAL PAGE IS
OF POOR QUALITY

- Wilhelms, D. E. (1973) Geologic map of the northern Crisium region: Apollo 17 preliminary science report, NASA Spec. Publ. SP-330, 29-29--29-35.
- Wilhelms, D. E. and McCauley, J. F. (1971) Geologic map of the near side of the moon: U. S. Geol. Surv. Misc. Inves. Map I-703.
- Wise, D. U. and Gates, M. T. (1970) Mascons as structural relief on a lunar 'Moho': J. Geophys. Res., 75, 261-268.
- Wood, J. A. (1970) Petrology of the lunar soil and geophysical implications: J. Geophys. Res., 75, 6497-6513.
- Zisk, S. H., Pettengill, G. M., and Catuna, G. W. (1974) High-resolution radar maps of the lunar surface at 3.8 cm wavelength: Moon, 10, 17-50.

ORIGINAL PAGE IS
OF POOR QUALITY

TABLES

TABLE I. Average surface elevation (in meters) of mare basin edge and interior based on control points used in construction of the isopach maps. The interior of mare surface is almost always depressed relative to the outer edge.

TABLE II. Comparison of surface depressions with basalt thickness and gravity anomalies. The basalt surface is usually depressed in areas of thick basalts. Gravity increases are associated with basalt thickness greater than 1000 m.

TABLE III. Average thickness of mare basalt in the shallow mare basins.

PRECEDING PAGE BLANK NOT FILMED

TABLE I

<u>BASIN</u>	<u>AVERAGE BASIN EDGE</u>	<u>AVERAGE INTERIOR</u>
SERENITATIS	4850	4627
SINUS AMORIS	5945	5978
TRANQUILLITATIS	6155	5852
TORRICELLI REGION	5244	5125
NECTARIS	5717	4950
CRISIUM	3905	3730
FECUNDITATIS	5452	5290
UNDARUM	6550	4815
SPUMANS	5936	5739
SMYTHII	3650	3617

TABLE II

<u>BASIN</u>	<u>SURFACE DEPRESSION</u>		<u>BASALT THICKNESS</u>		<u>GRAVITY</u>	
	<u>Location</u>	<u>Local Relief</u>	<u>Total</u>	<u>Local Express</u>	<u>Location</u>	<u>Anomaly</u>
Serenitatis	27°N; 25°E	200 m	>1.5 km	>1.5 km	23°N; 18°E	160
	20°N; 27°E	125	>1.0	0.5	-None	-
Sinus Amoris	16°N; 37°E	150	0.75	0.5	-None	-
Tranquillitatis	13°N; 31°E	_____	1.0	0.75	-None	-
	7°N; 39°E	_____	0.75	0.50	-None	-
	5°N; 22°E	300	1.25	0.50	5°N; 23°E	40
	5°S; 30°E	300	1.25	0.50	7°S; 27°E	40
Nectaris	-Not Measured-		>1.5	>1.5	14°S; 33°E	100
Crisium	18°N; 54°E	300	>1.5	>1.5	17°N; 55°E	120
Fecunditatis	4°N; 49°E	200	0.5	0.25	-None	-
	2°N; 58°E	150	0.5	0.25	-None	-
	0°; 54°E	250	0.25	0	-None	-
	3°S; 52°E	300	>1.5	0.75	2°S; 52°E	40
	5°S; 60°E	400	0.5	0.5	-None	-
Smythii	2°N; 85°E	300	0.5	0.5	2°S; 84°E	80

TABLE III

<u>BASIN</u>	<u>AREA</u> (X 10 ⁴ km ²)	<u>VOLUME</u> (X 10 ³ km ³)	<u>AVERAGE THICKNESS</u> (in meters)
Serenitatis			
Sinus Amoris	4.1	816	210
Tranquillitatis	43	199	460
Nectaris*	25	120	470
Crisium			
Fecunditatis	40	127	320
Undarum	34	6.6	190
Spumans	18.6	3.9	210
Smythii	39	9	230

*Nectaris data includes trough between 2⁰-10⁰ S.

ILLUSTRATIONS

- Figure 1. Crater depth of rim height relations for fresh appearing lunar craters (Pike, 1972).
- Figure 2. Estimation of mare basalt thickness in the vicinity of a flooded crater. The thickness determined does not include the thick interior lens.
- Figure 3. Location of interior data points used in the construction of the isopach map.
- Figure 4. Surface topography of the maria. Contour interval is 500 m. Highland areas between basins are not contoured.
- Figure 5. Isopach map of the eastern mare basalts. Isopach interval is 250 m. Stippled areas are outside the area of topographic coverage.
- Figure 6. Structural map of the basins' floors. Contour interval is 500 m. Interbasinal highlands are not contoured.
- Figure 7. Surface features of Mare Serenitatis. Mare ridges are shown by line with double barb; rilles by line and dot.
- Figure 8. TOP (a) Generalized surface topography of the Serenitatis basin. Contour interval is 250 m.
MIDDLE (b) Isopach map of Mare Serenitatis basalts. Isopach lines are at 250 m intervals. Crosses mark location of thickness estimates.

BOTTOM (c) Structural contours on the floor of the Serenitatis basin. Contour interval is 250 m. Data is insufficient to construct midbasin configuration.

Figure 9. Surface features of Mare Tranquillitatis. Mare ridges are shown by line with double barb; rilles by line and dot; mare domes by ellipses.

Figure 10. Isopach map of Mare Tranquillitatis and Sinus Amoris. Isopach interval is 250 m. Thickest basalts occur in the region of Lamont.

Figure 11. Surface features of Mare Nectaris. Mare ridges are shown by line with double barb; rilles by line and dot; mare domes by ellipses, large buried craters by closed dash and dot line.

Figure 12. TOP (a) Generalized surface topography in trough between Mare Nectaris and Mare Tranquillitatis. Contour interval is 250 m. Surface elevations are not available for the surface of Mare Nectaris.

BOTTOM (b) Structural contours beneath mare basalts in region depicted in (a) above. Contour interval is 250 m.

Figure 13. Isopach map of the Mare Nectaris region. Isopach lines are at 250 m interval. Thick basalts within the trough coincide with the region of Torricelli R. The thick lens within the Nectaris

basin is constructed by projecting thicknesses toward the region of maximum gravity anomaly.

Figure 14. Surface features of Mare Crisium. Mare ridges are shown by line with double barb; mare domes by ellipses.

Figure 15. TOP (a) Generalized surface topography of southern Mare Crisium. Contour interval is 250 m. Central Mare Crisium is essentially flat at this contour interval.

BOTTOM (b) Structural contours on the floor of the Crisium basin. Contour interval is 250 m.

Figure 16. Isopach map of southern Mare Crisium basin. Isopach lines are at 250 m intervals. Crosses mark the location of thickness estimates. Thickest basalts (greater than 1000 m) are determined by projection.

Figure 17. Surface features of Mare Fecunditatis. Mare ridges are shown by line with double barb; rilles by line and dot. Note pattern of mare ridges and location of the central Fecunditatis gravity anomaly.

Figure 18. Generalized surface topography of northern Mare Fecunditatis. Contour interval is 250 m. Surface elevation data is not available for the southern part of the basin.

Figure 19. Isopach map of Mare Fecunditatis. Isopach lines are at 250 m interval. Crosses mark locations of interior data points used in the construction of the map.

Figure 20. Structural contours on the floor of the Fecunditatis basin. Contour interval is 250 m.

Figure 21. Generalized surface topography of the Mare Spumans and Mare Undarum region. Contour interval is 500 m with 250 m supplementary contours.

Figure 22. Isopach map of mare basalts in Mare Undarum (northeast) and Mare Spumans (southwest). Isopach lines are at 200 m intervals. Crosses mark locations of data points used in the construction of the isopach map.

Figure 23. Structural contours on the floors of the Undarum and Spumans basins. Contour interval is 500 m with 250 m supplementary contours.

Figure 24. Surface features of Mare Smythii. Mare ridges are shown by line with double barb. The basin floor is outlined with broken line. The mare basalts, enclosed in a solid line, are restricted to the northeastern portion of the basin.

Figure 25. TOP (a) Surface topography of northeastern Mare Smythii. Contour interval is 100 m.

MIDDLE (b) Isopach map of mare basalts in the Smythii basin. Isopach lines are at 2.50 m intervals.

BOTTOM (c) Structural contours beneath mare basalts in the Smythii basin. Contour interval is 250 m.

Figure 26. Generalized composite map of the surface features of the eastern mare basins. Mare ridges are shown by line with double barb; rilles by line with dot; mare domes by solid ellipses.

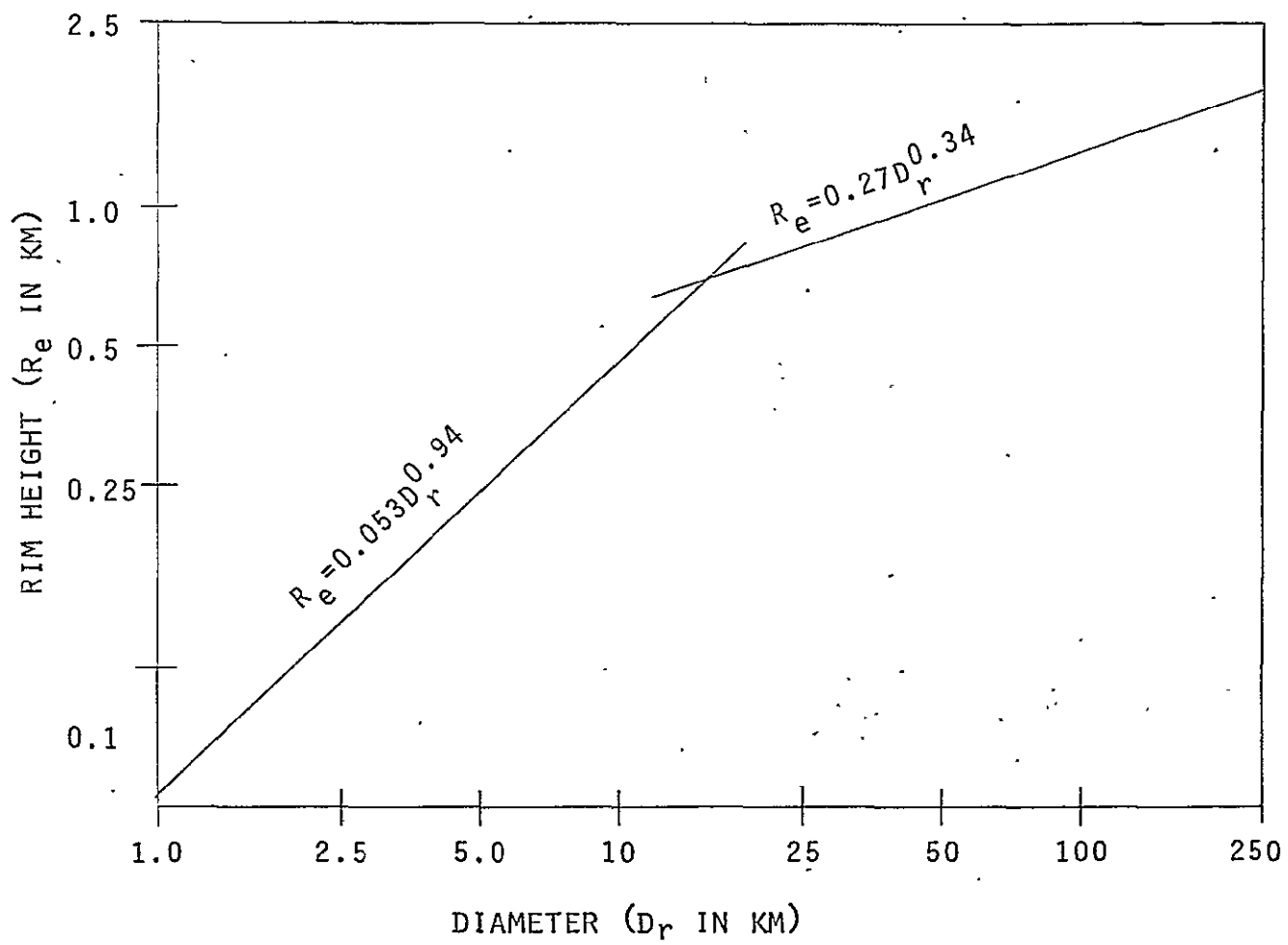
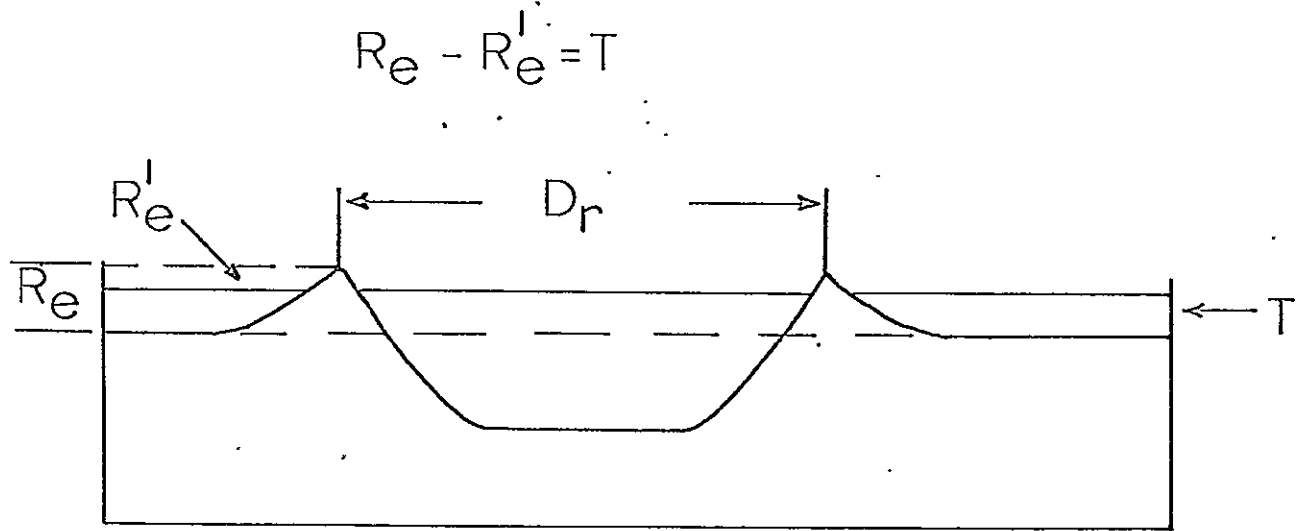


Figure 1



R_e = Rim Height

R_e' = Exposed Rim Height

T = Thickness of Mare

Figure 2

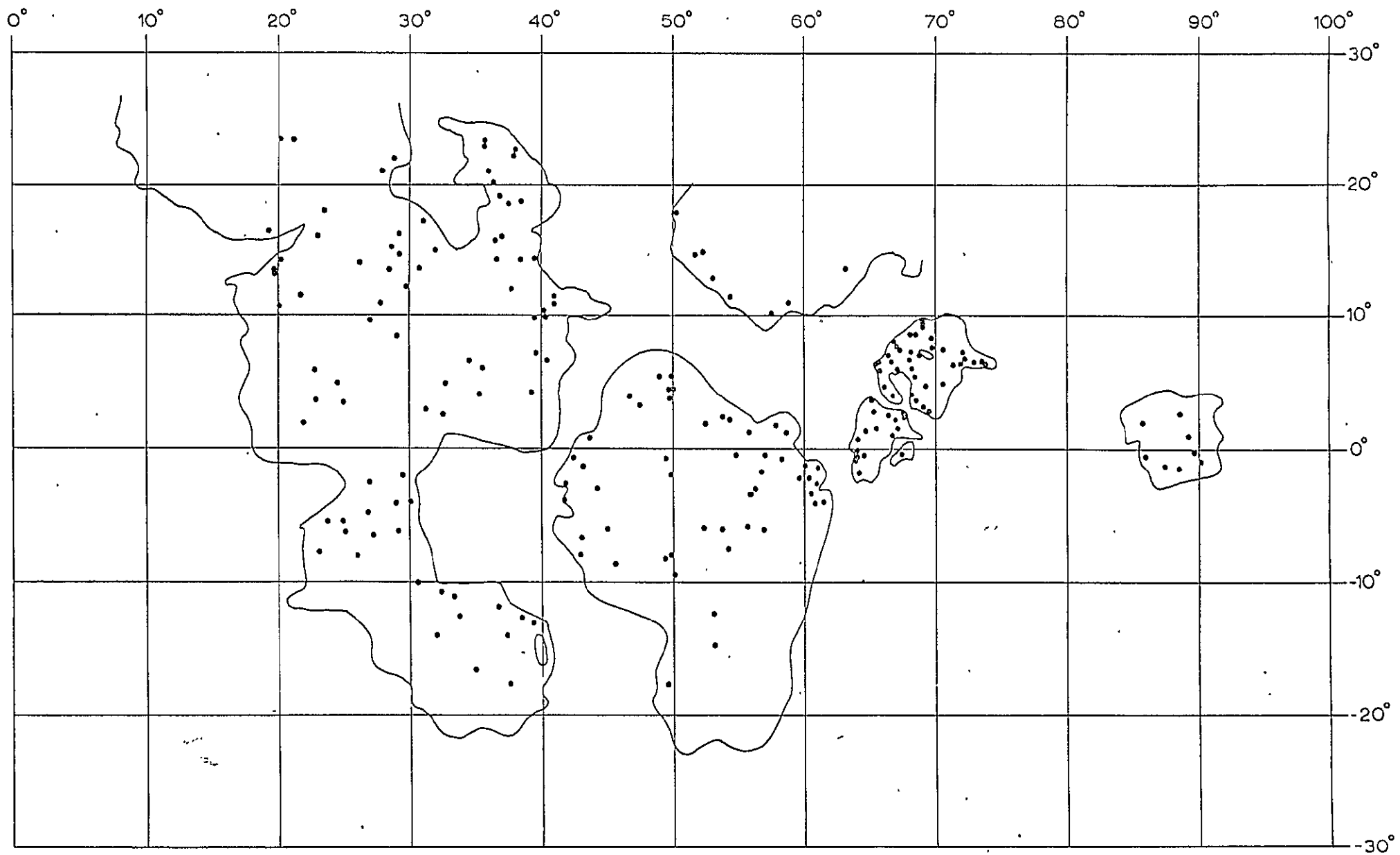


Figure 3

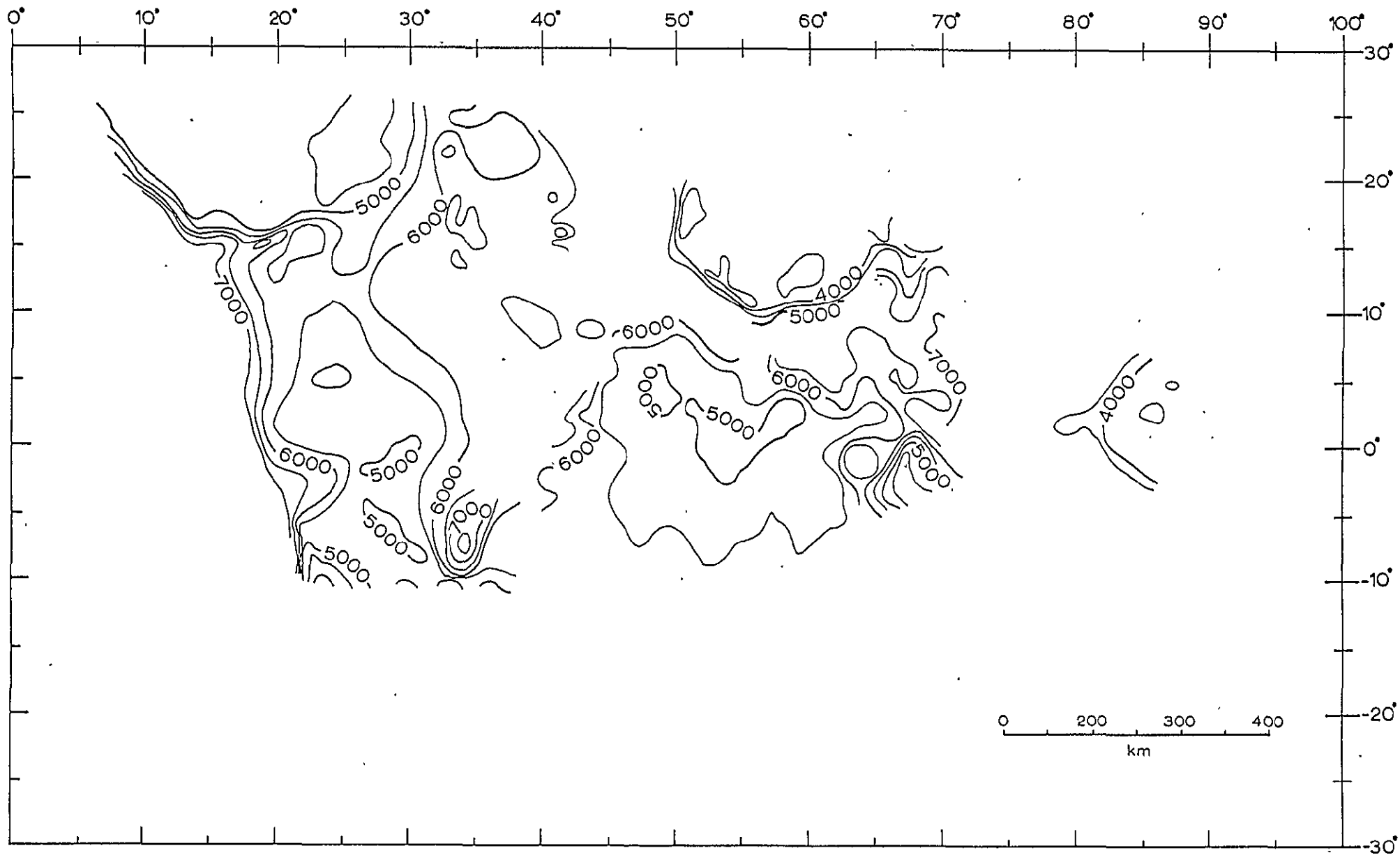


Figure 4

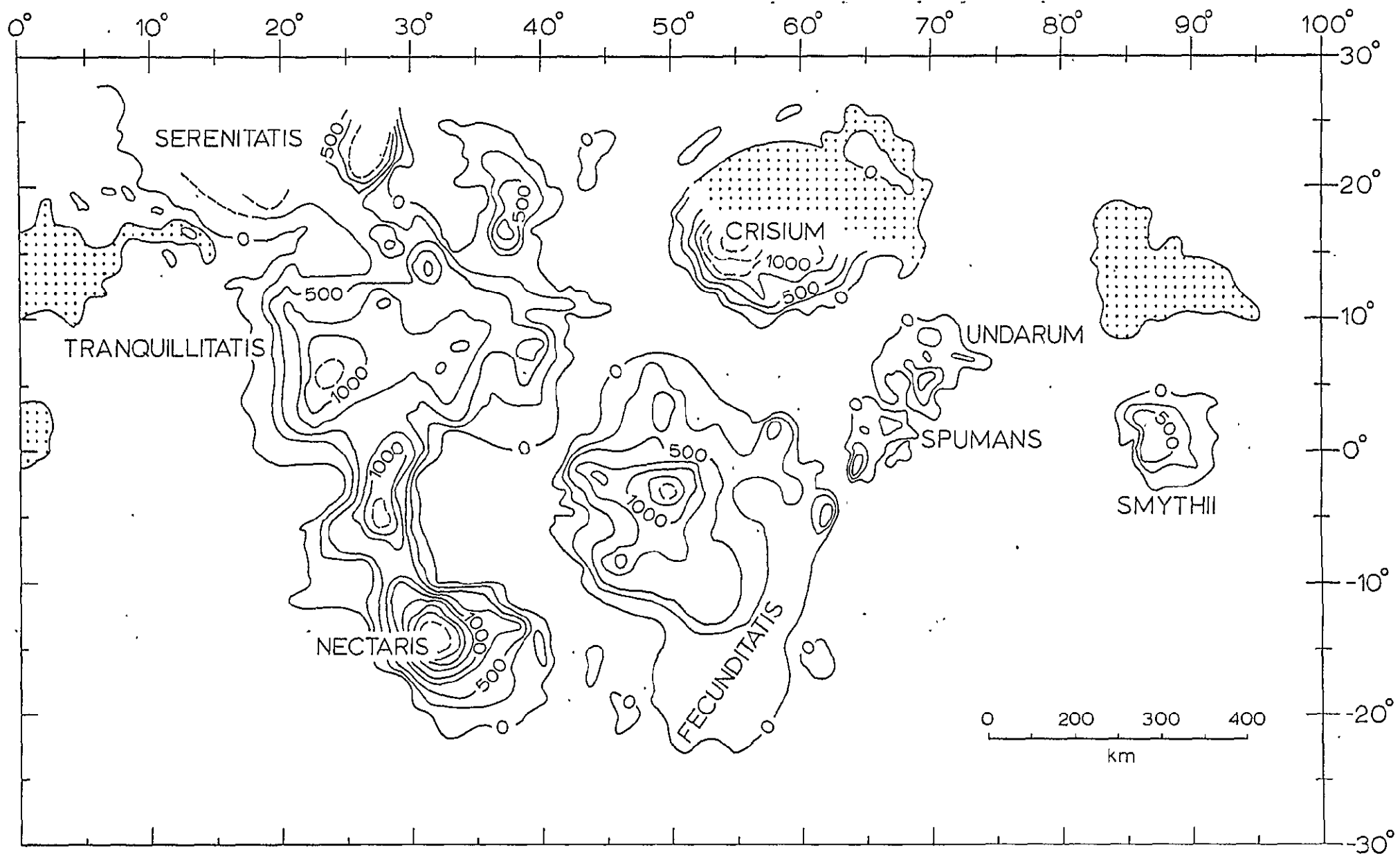


Figure 5

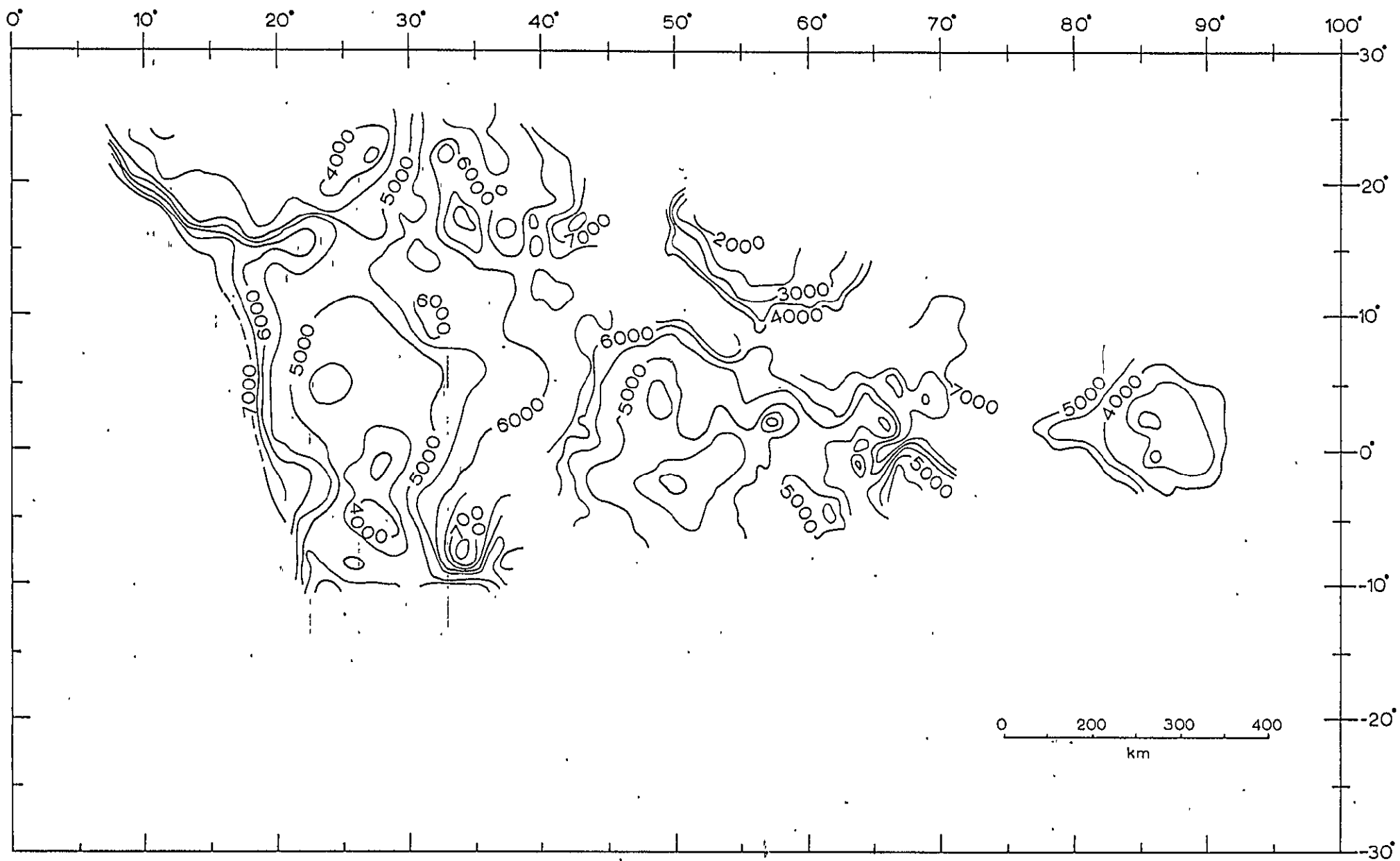


Figure 6

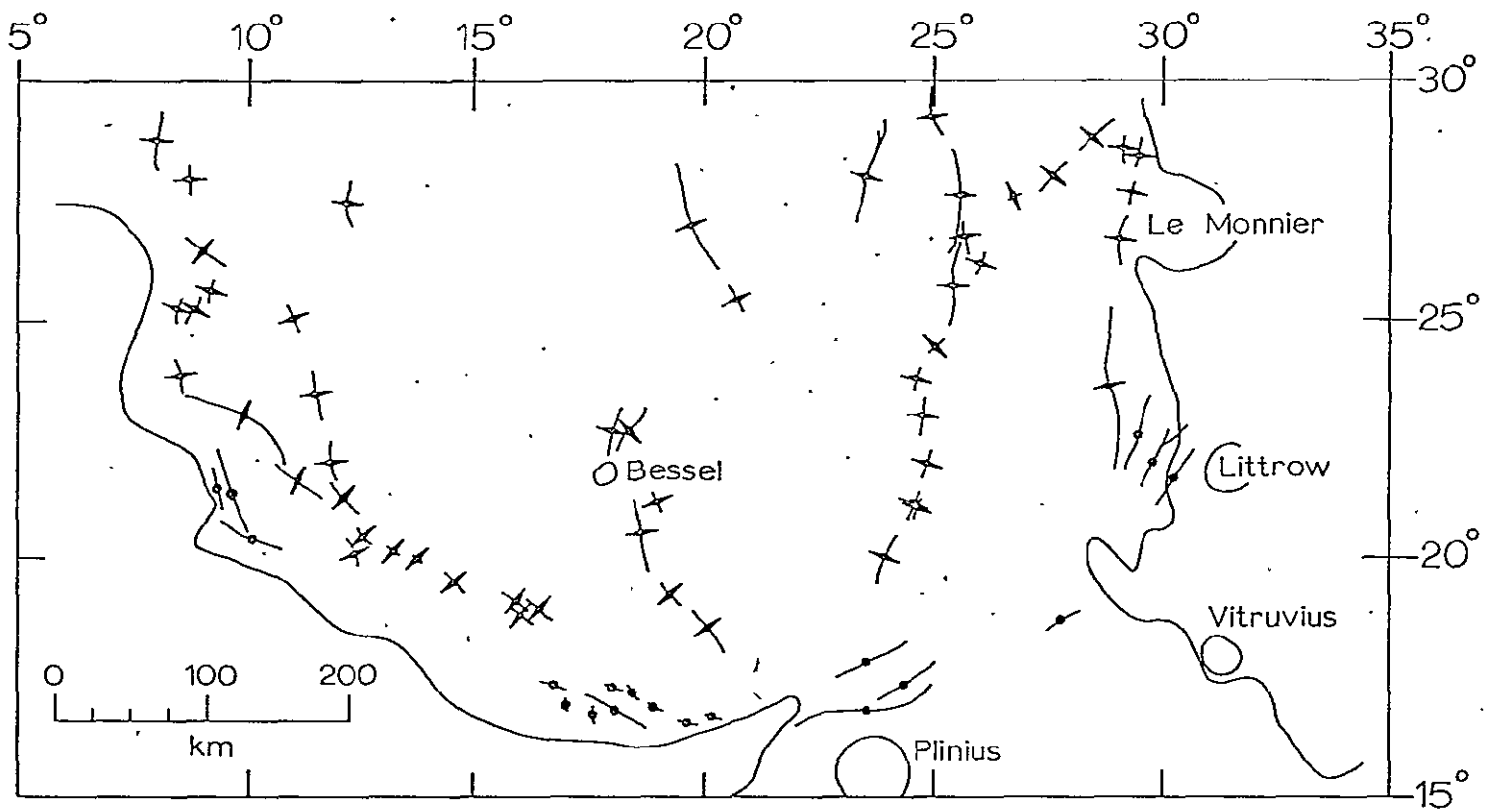
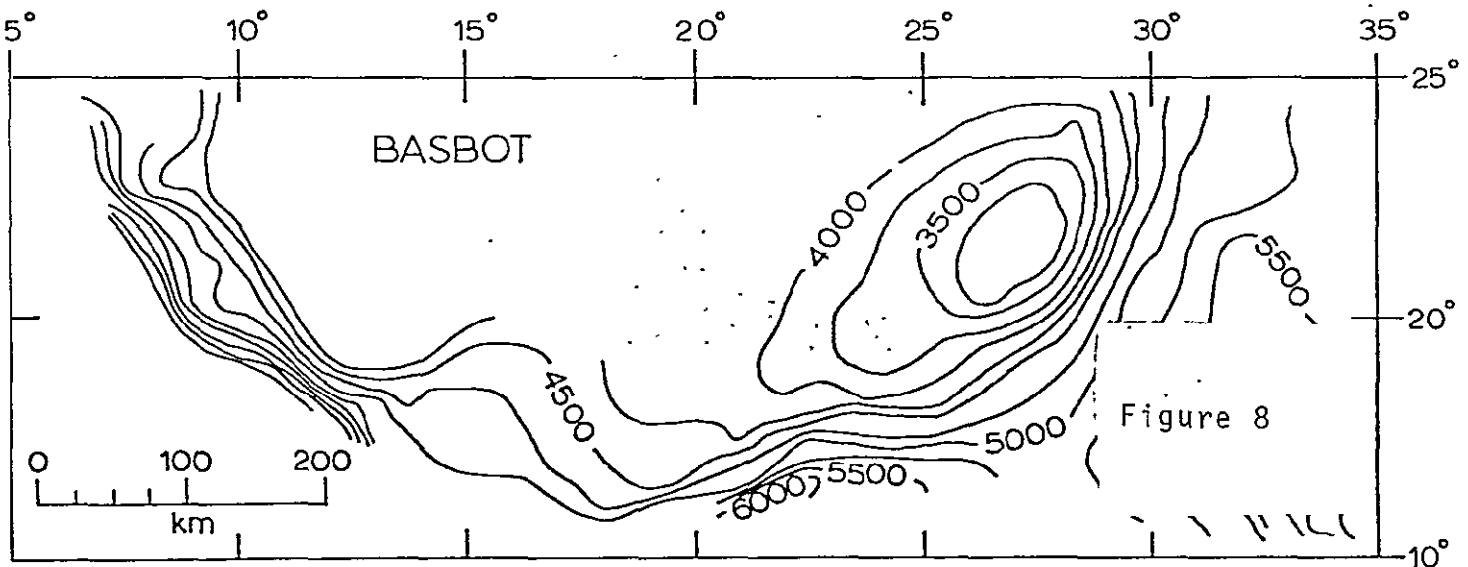
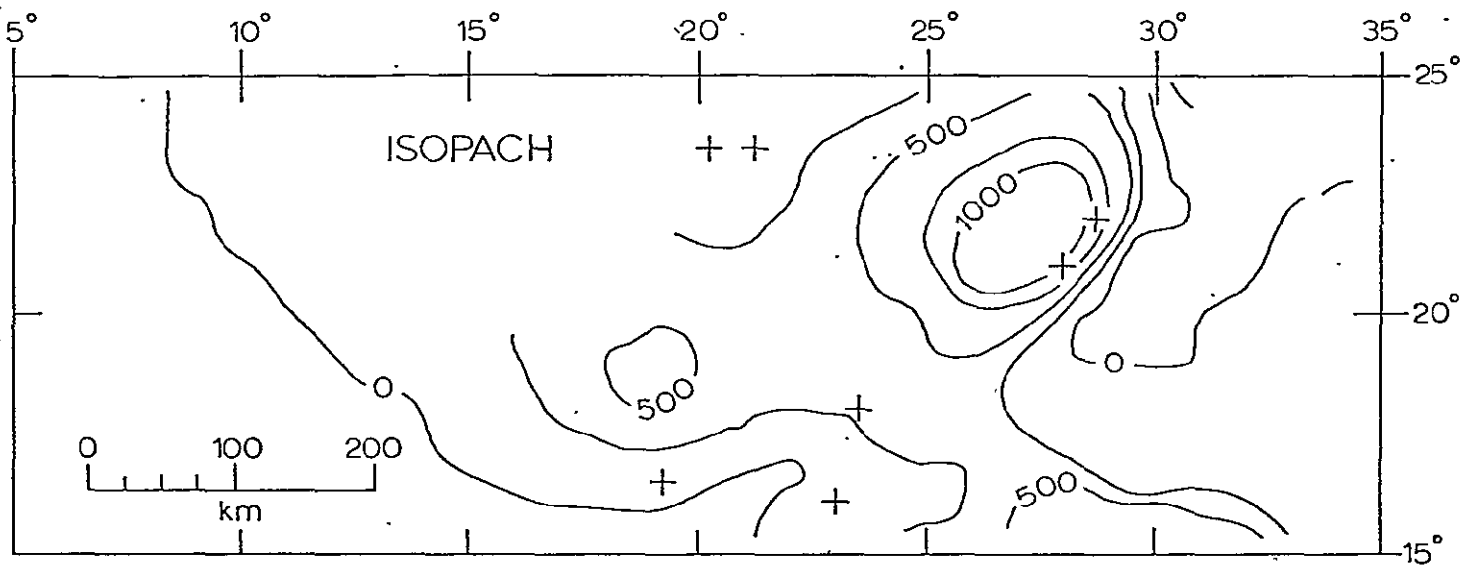
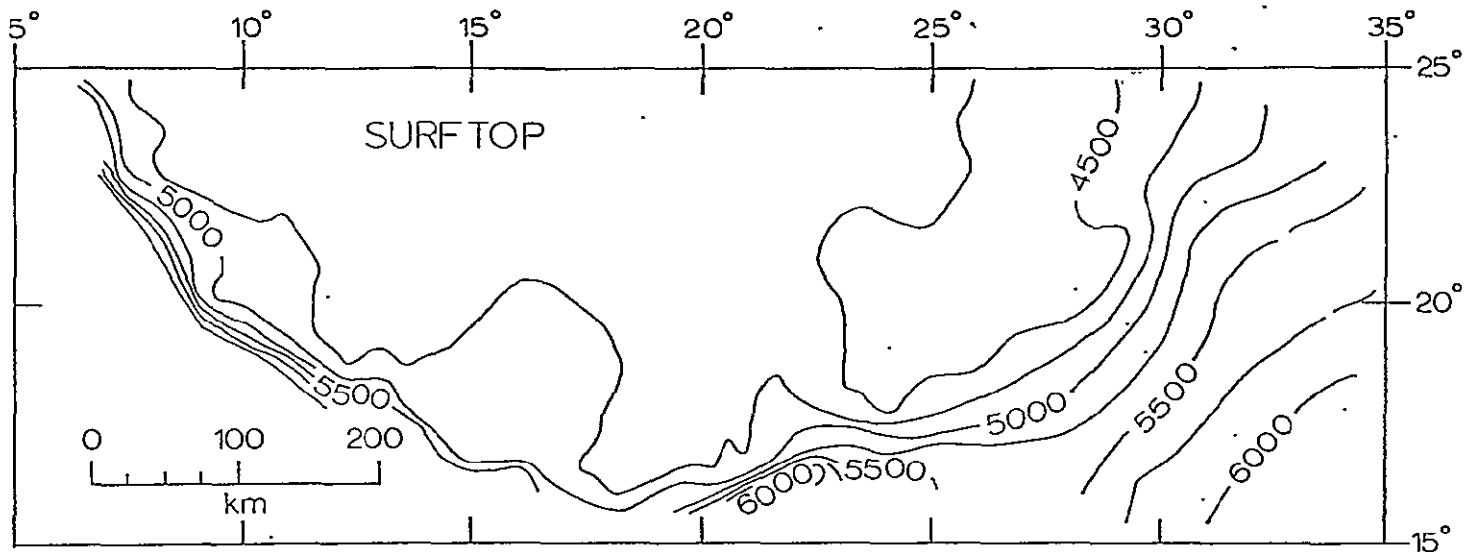


Figure 7



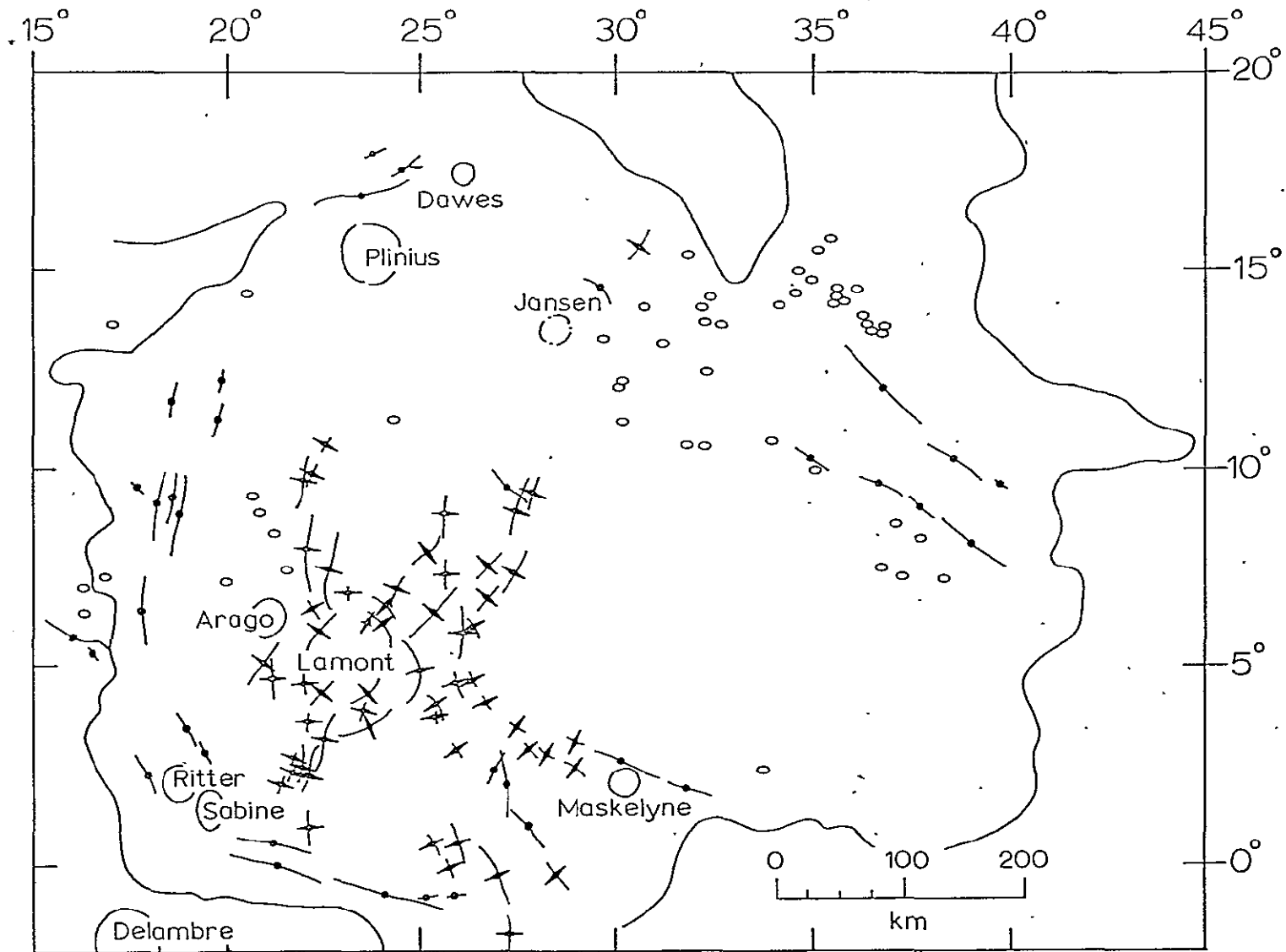


Figure 9

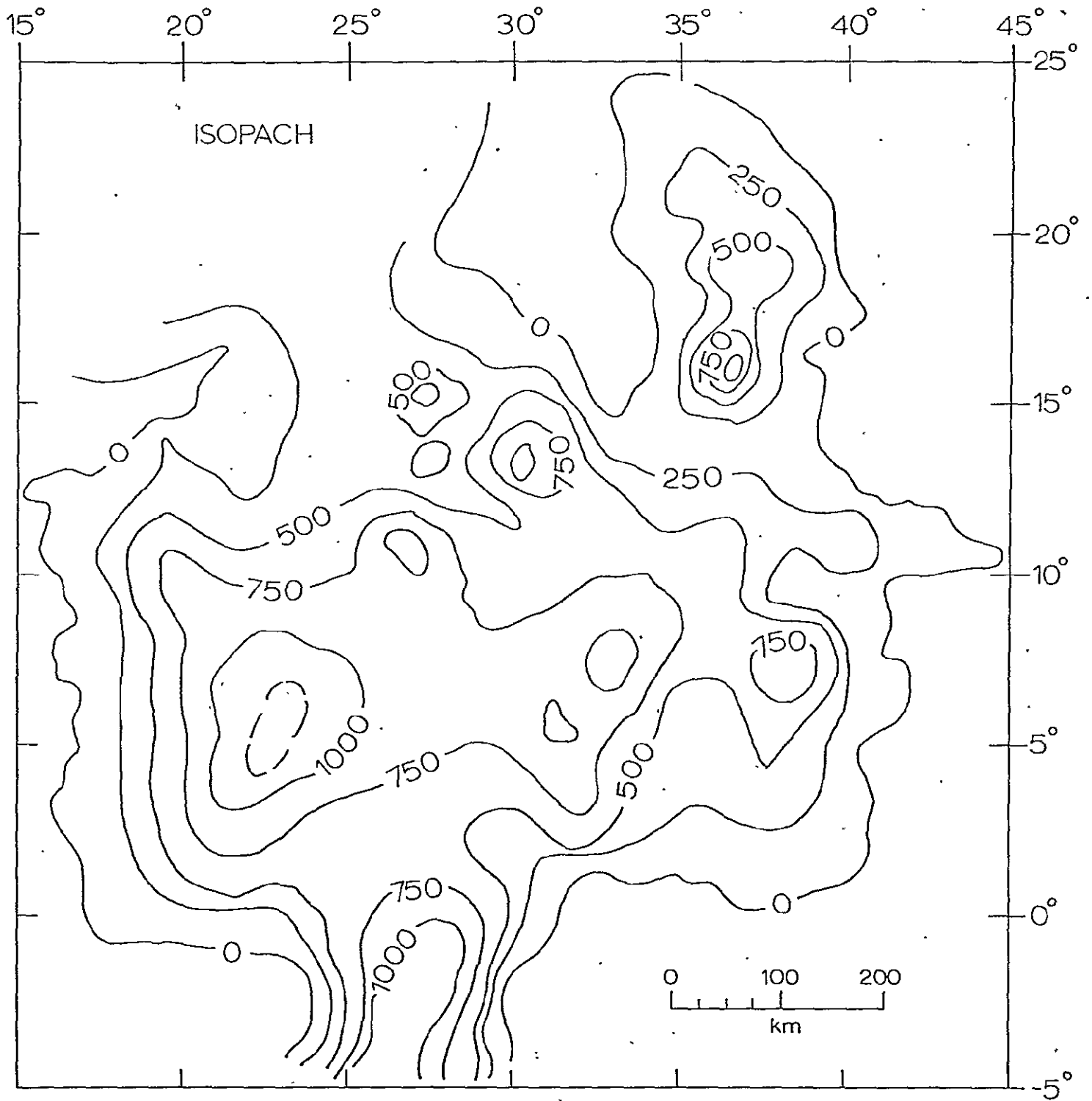


Figure 10

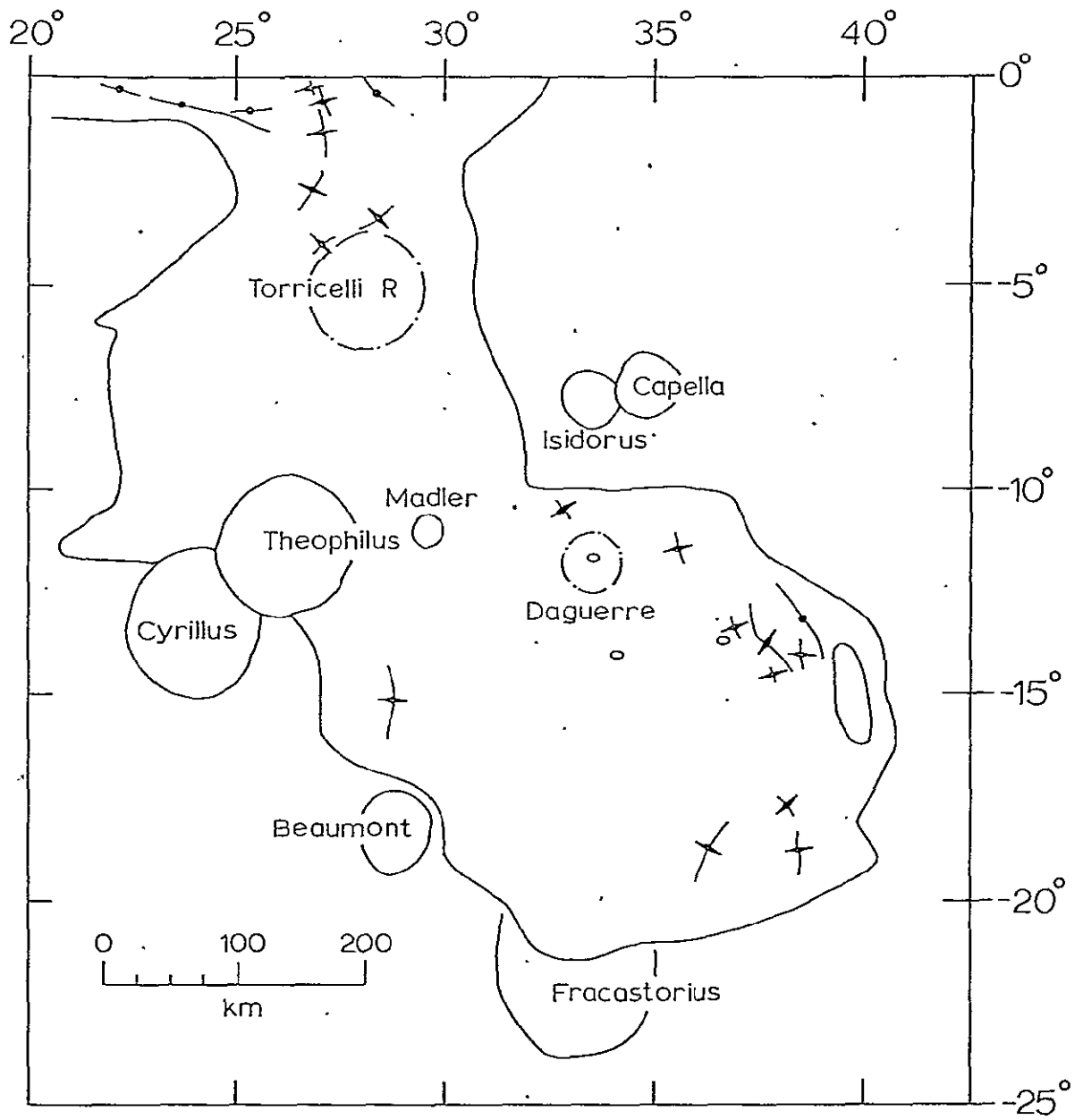


Figure 11

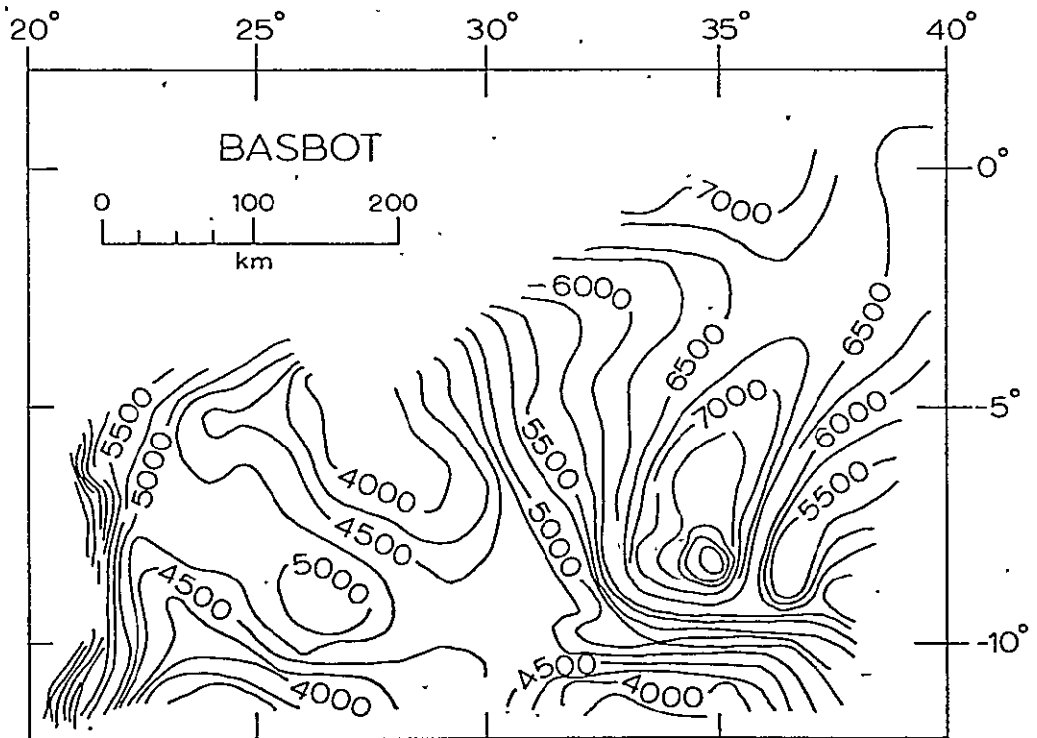
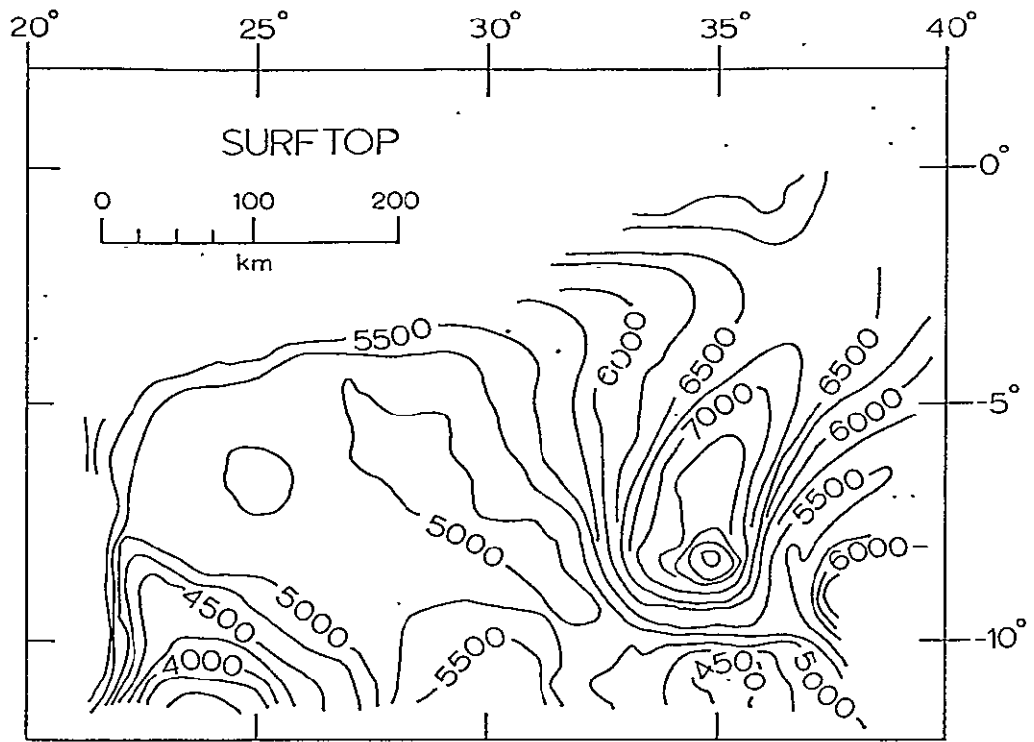


Figure 12

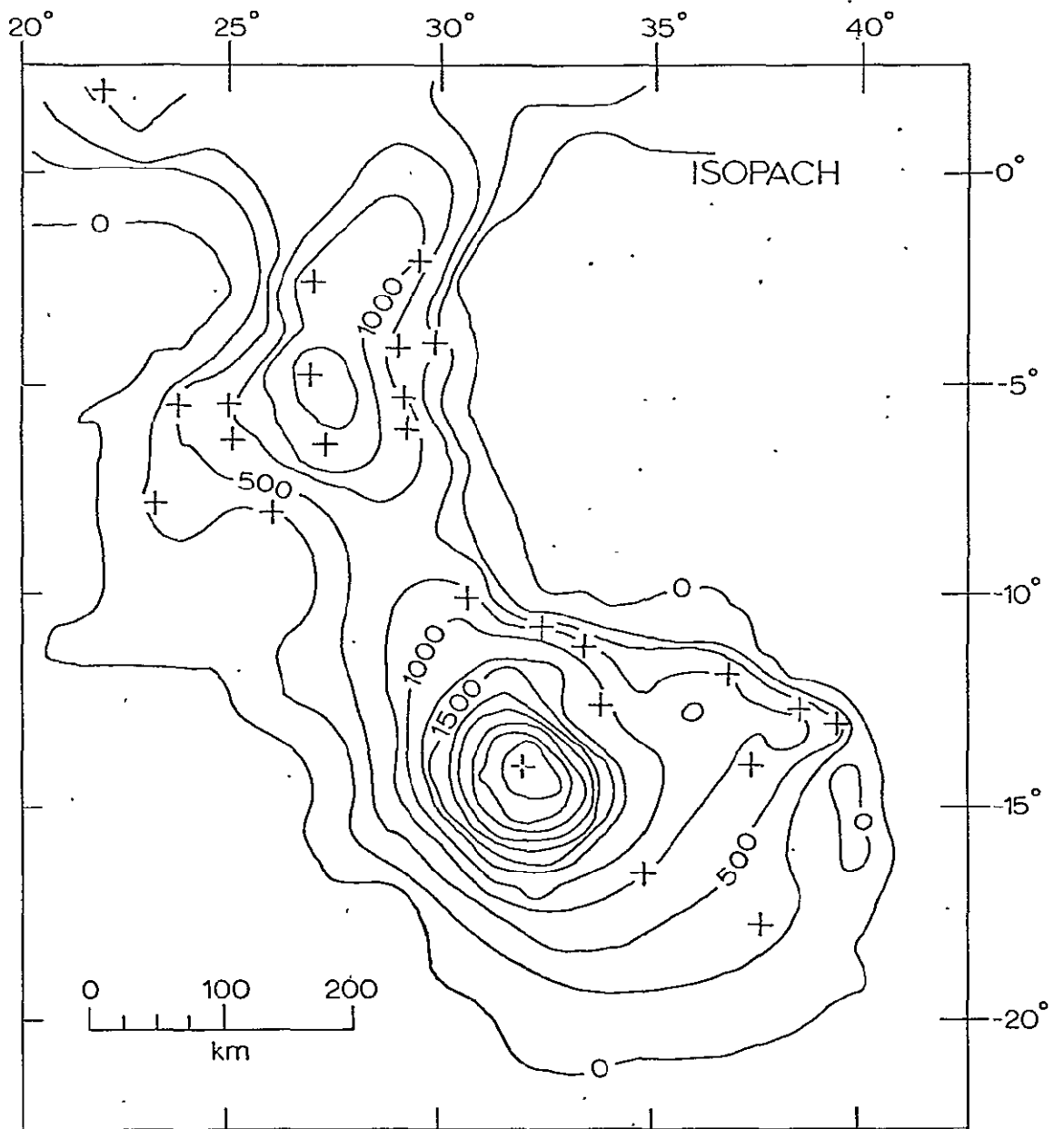


Figure 13

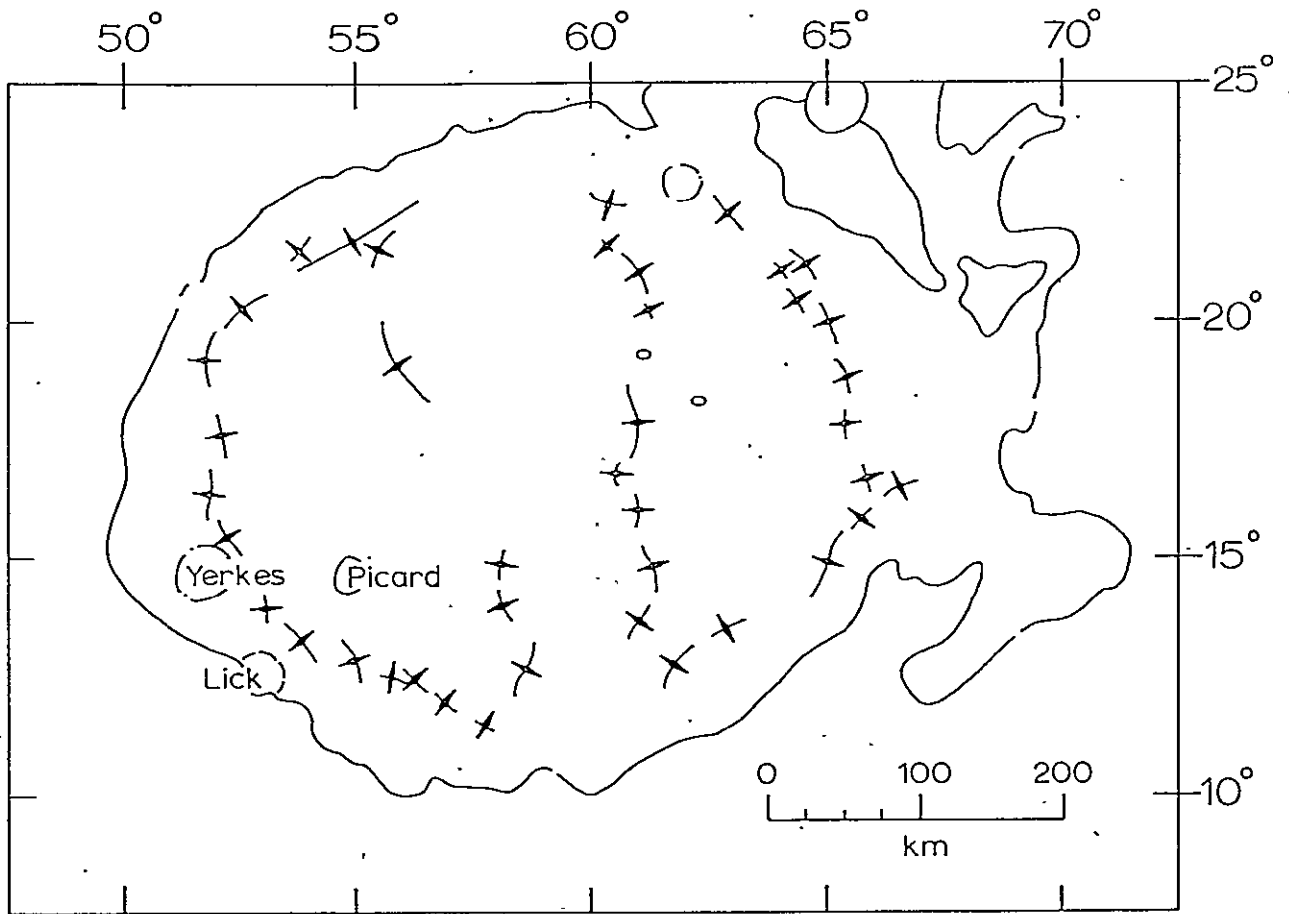


Figure 14

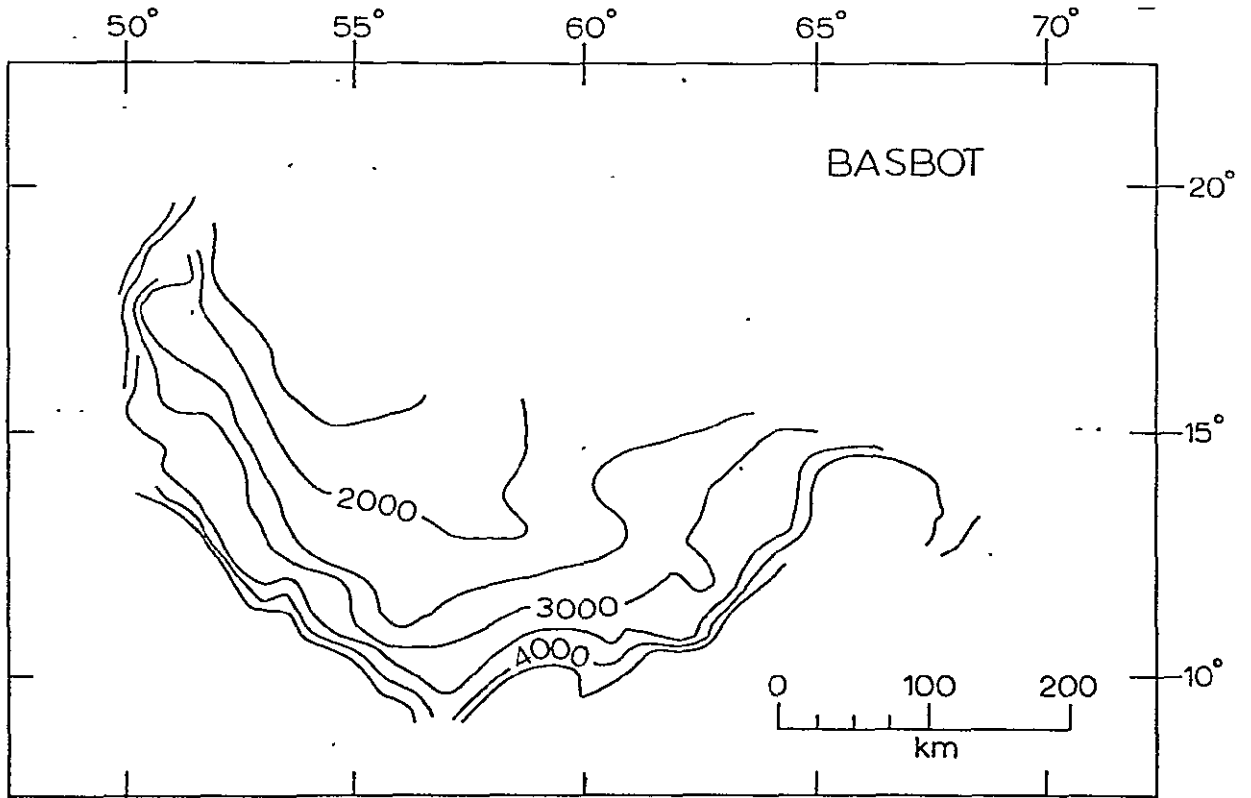
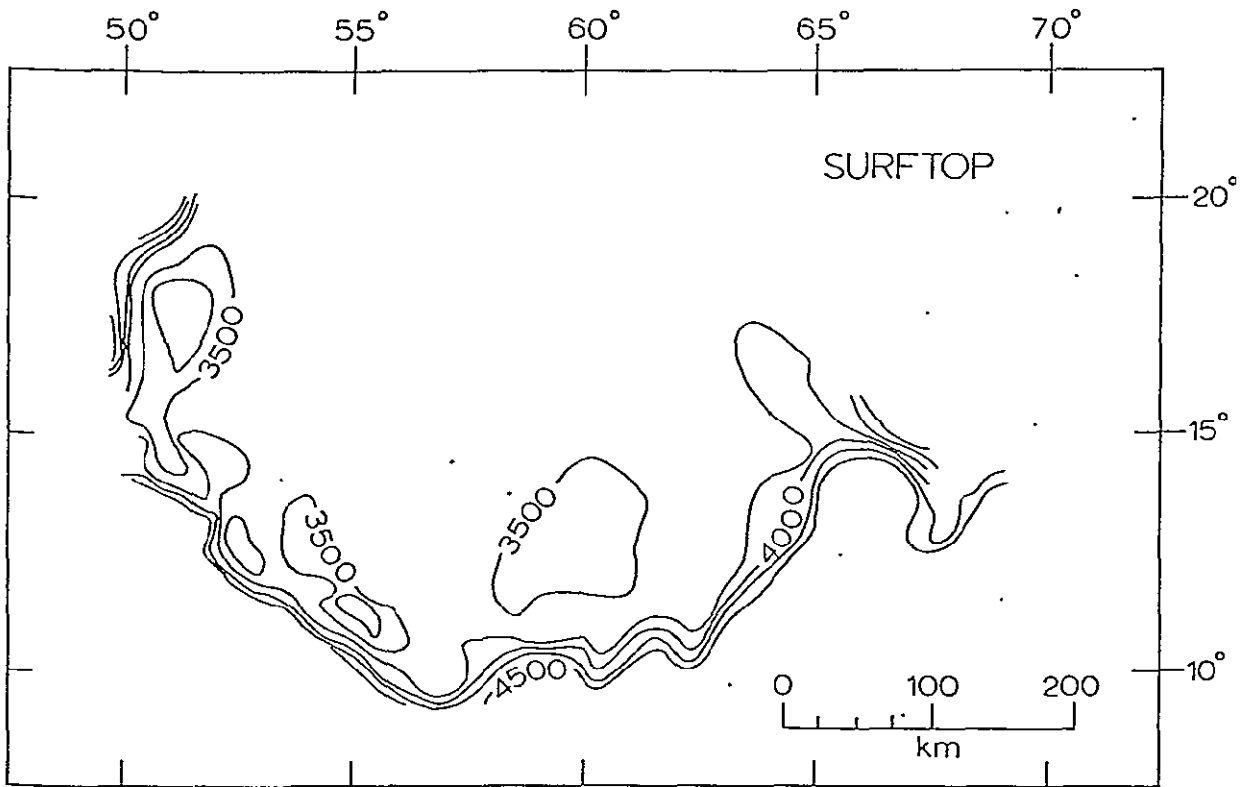


Figure 15

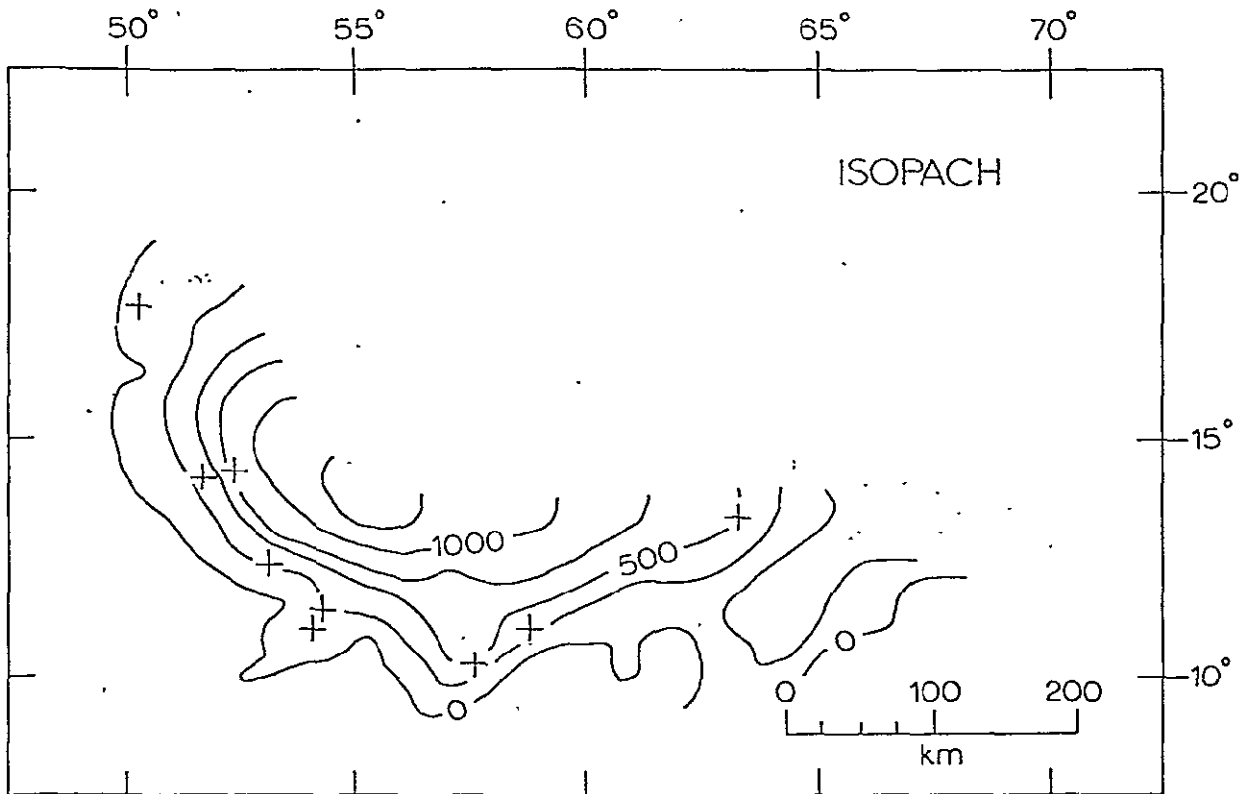


Figure 16

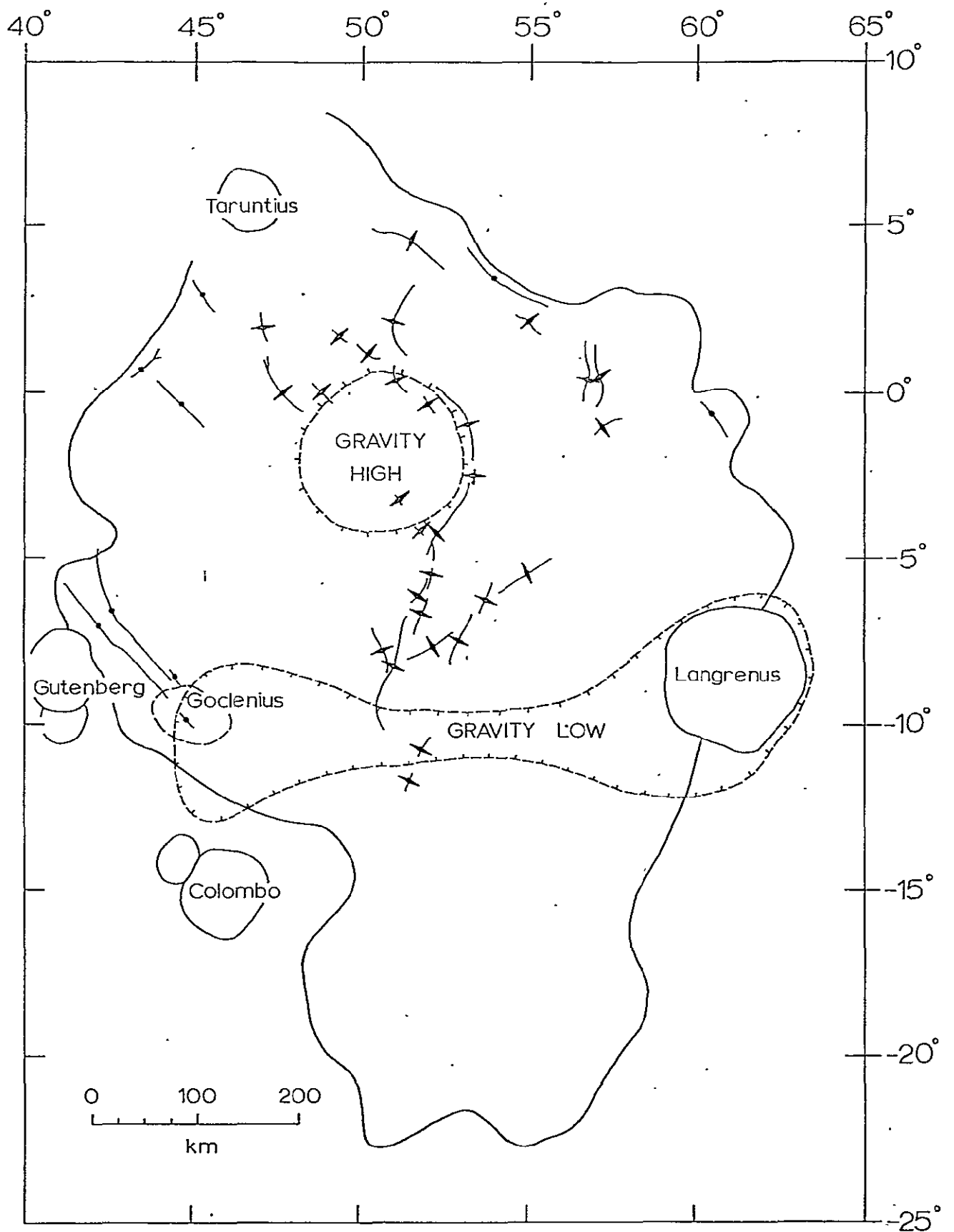
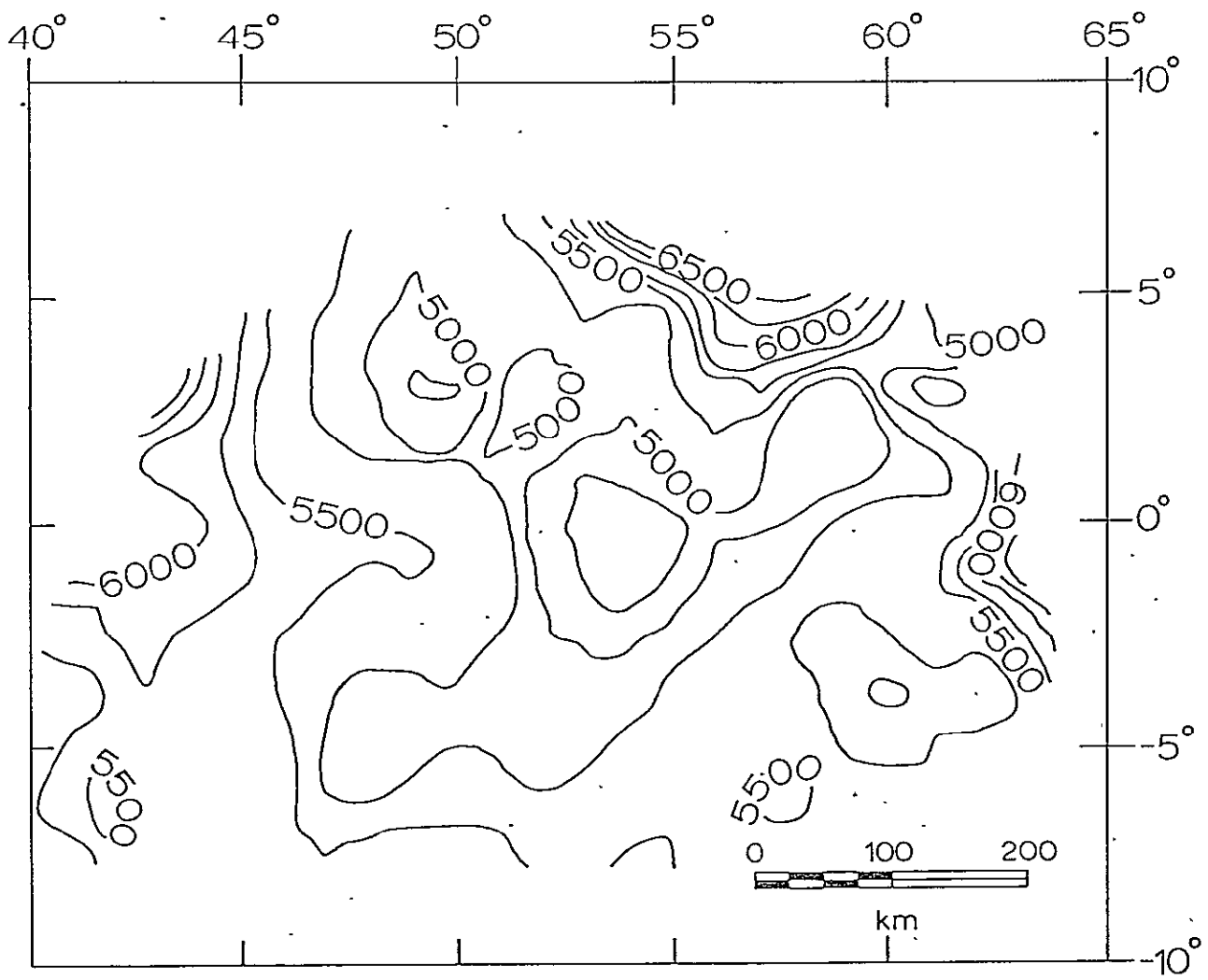


Figure 17



.Figure 18

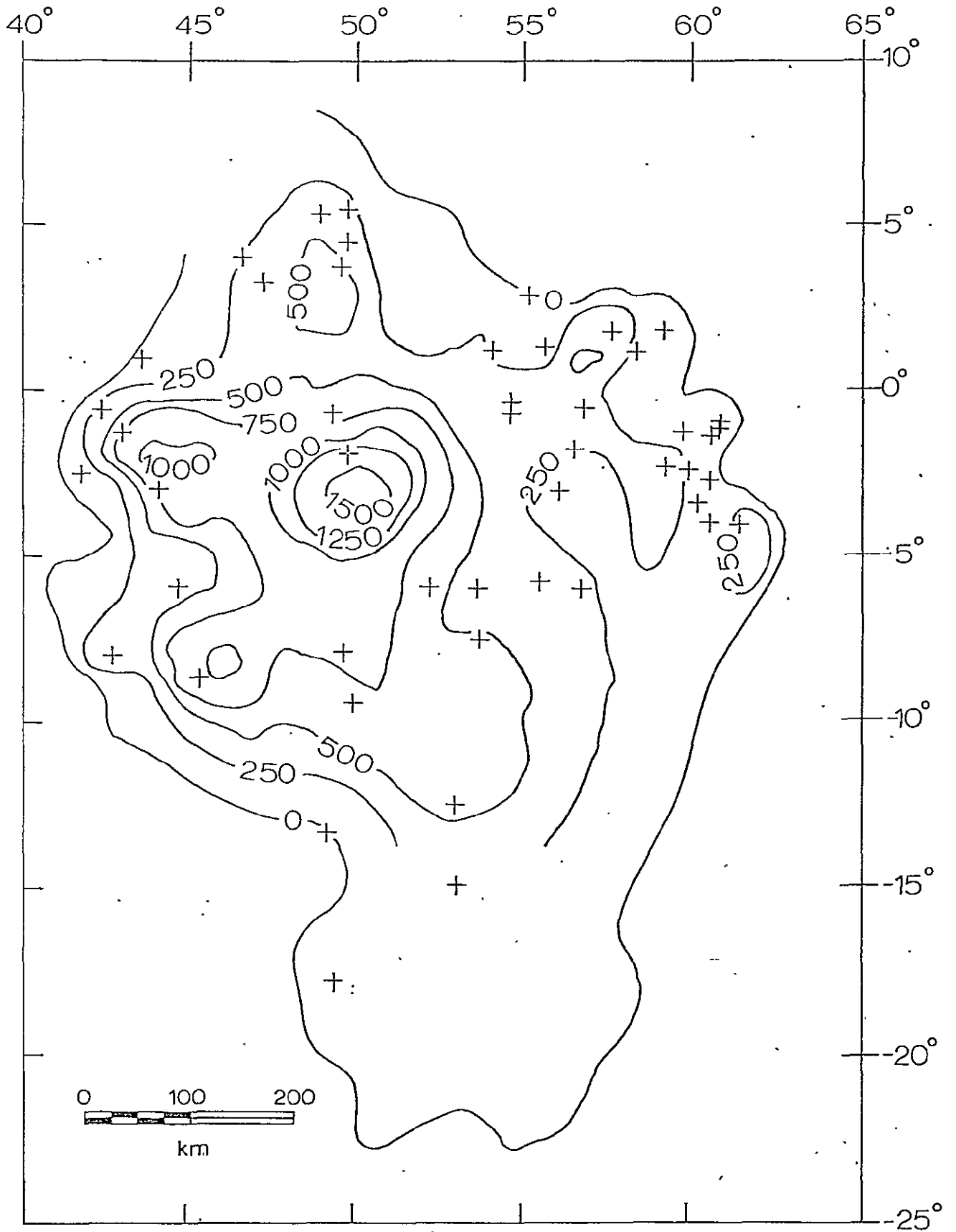


Figure 19

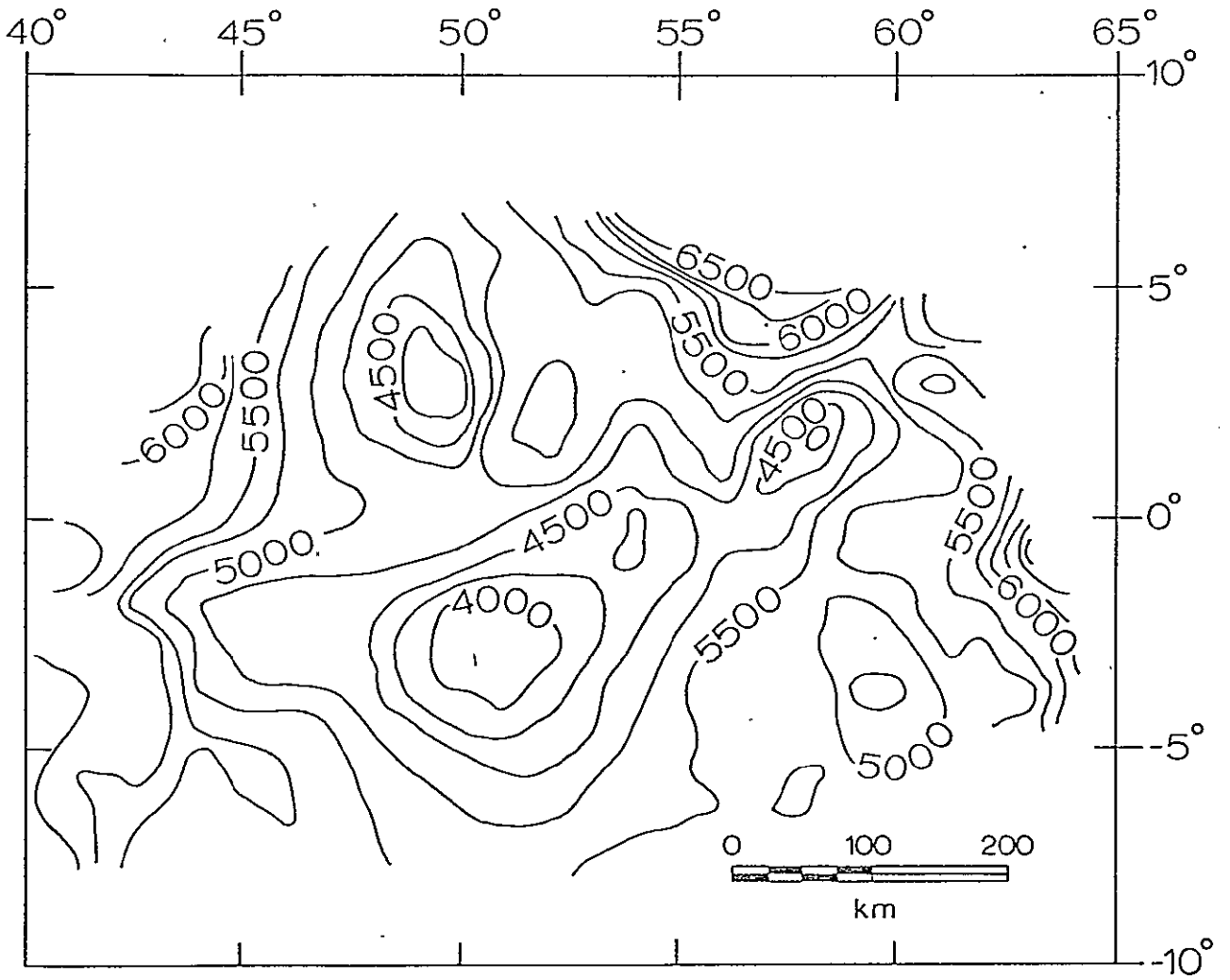


Figure 20

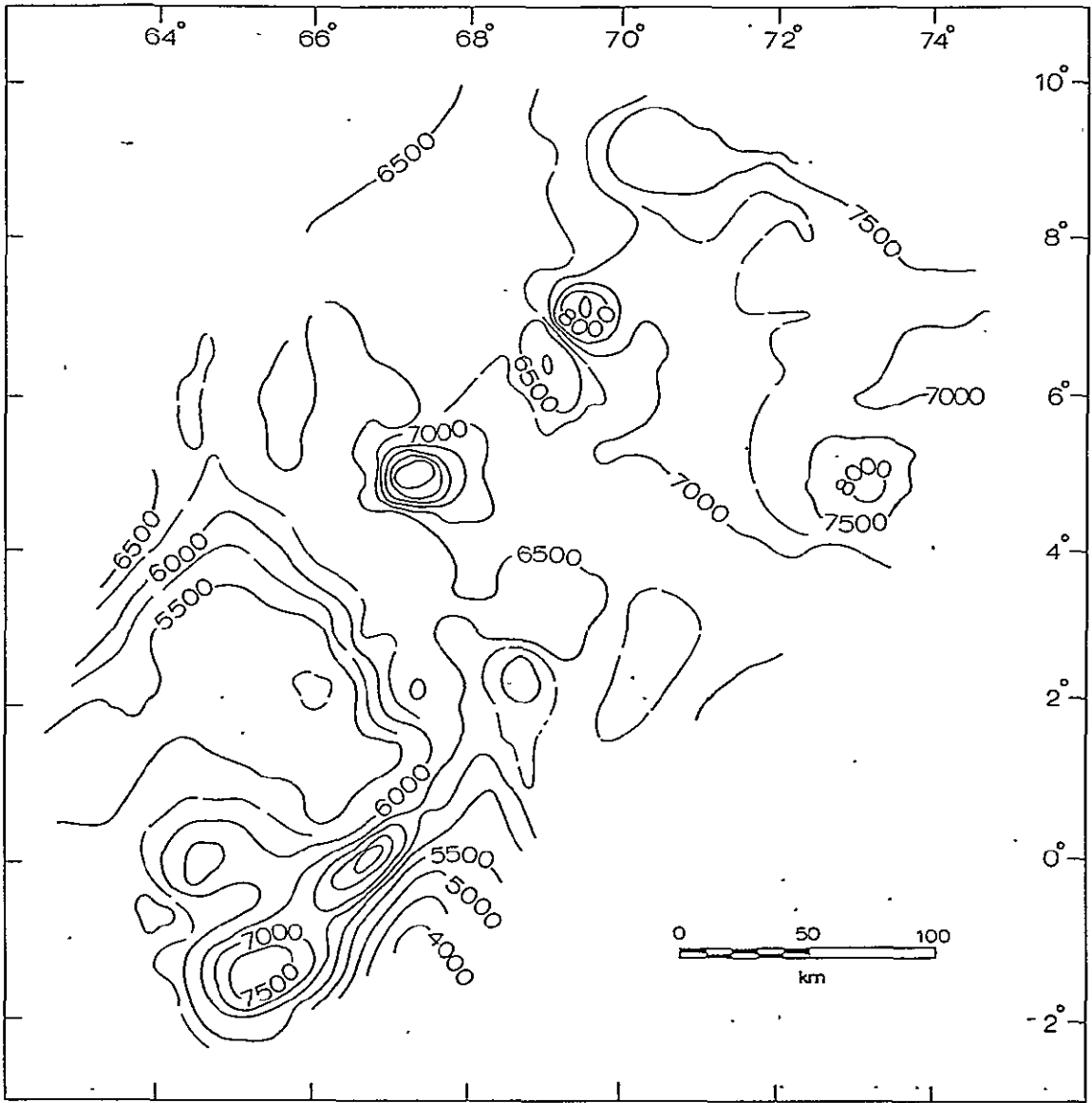


Figure 21

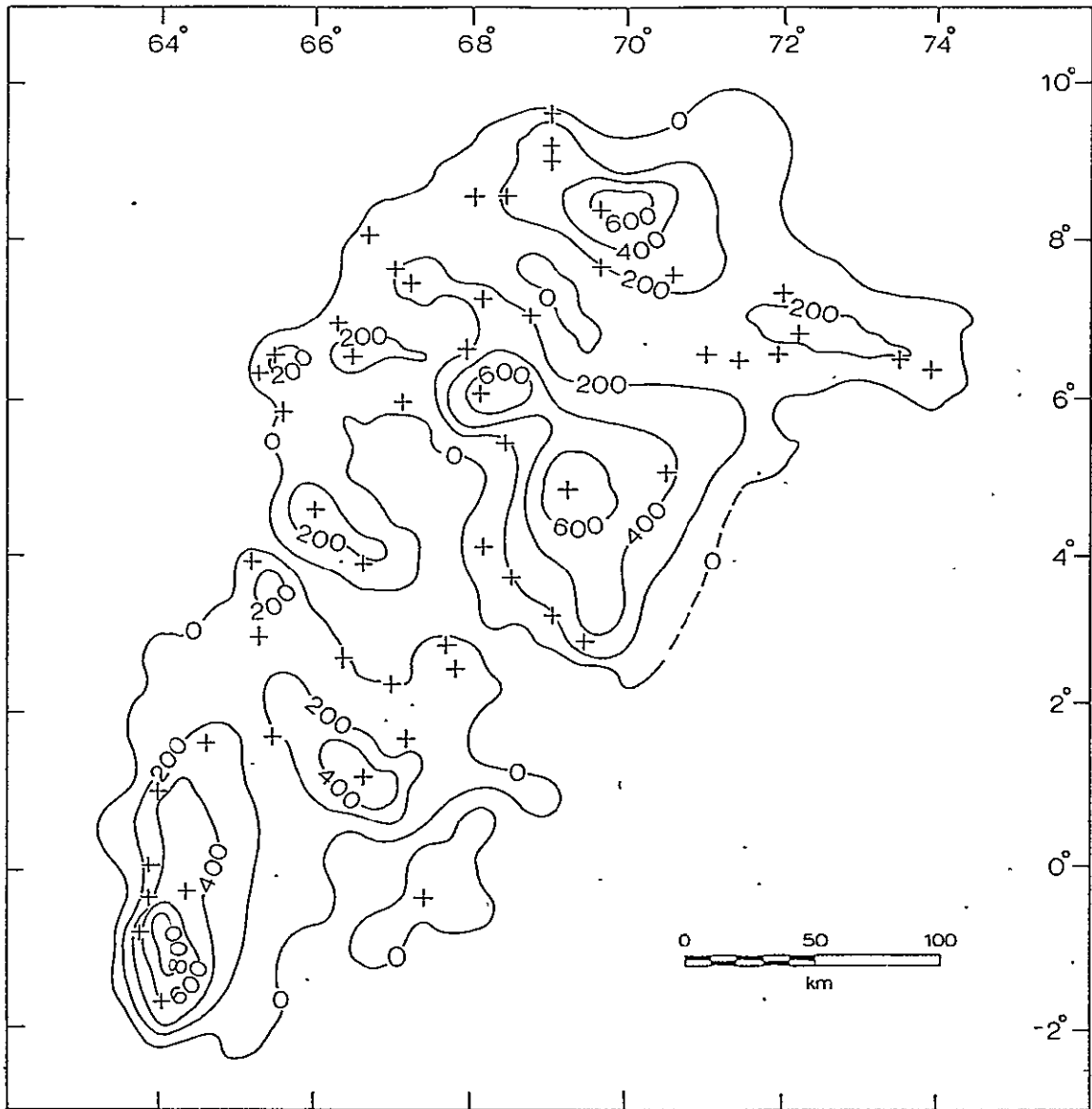


Figure 22

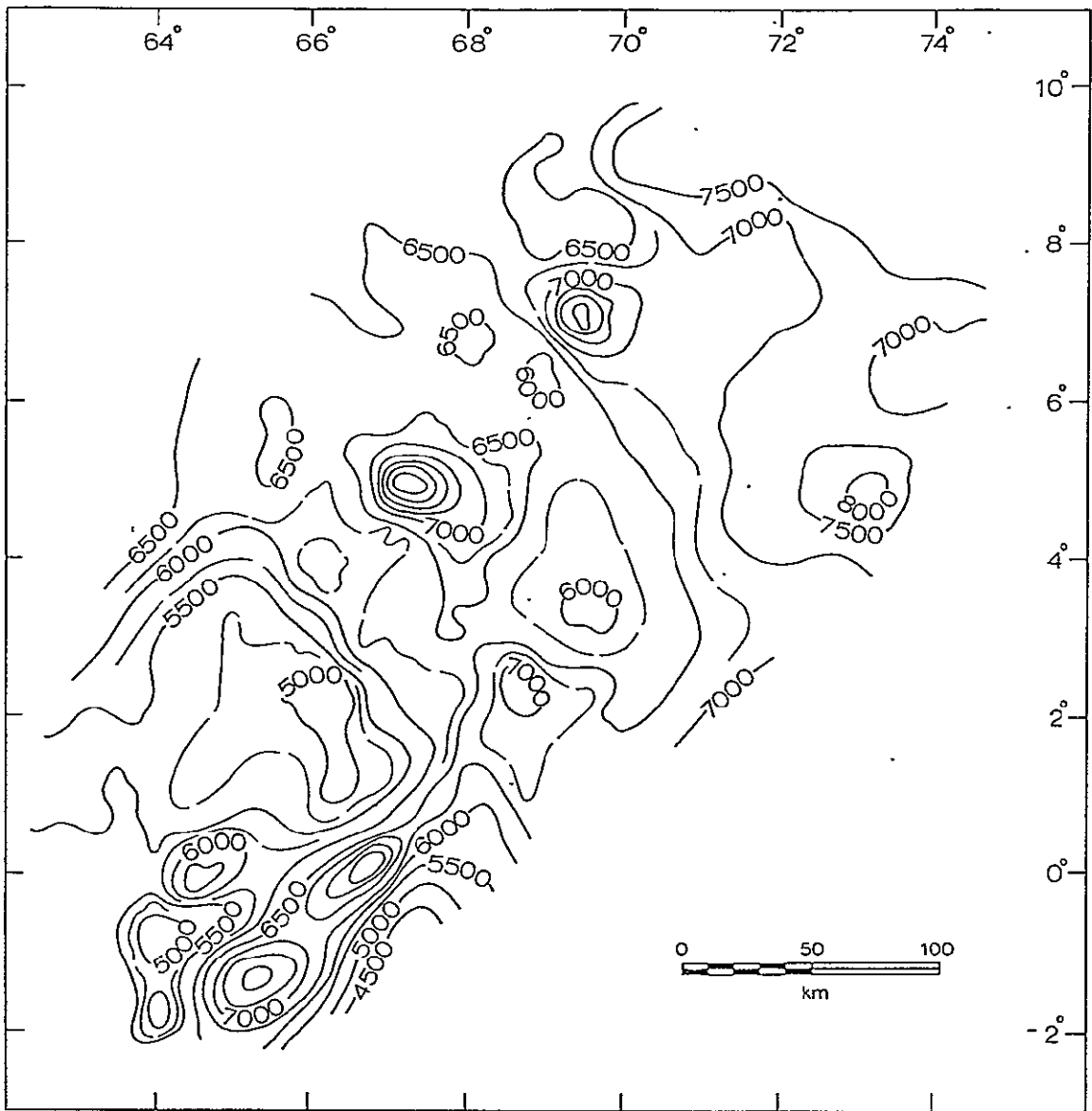


Figure 23

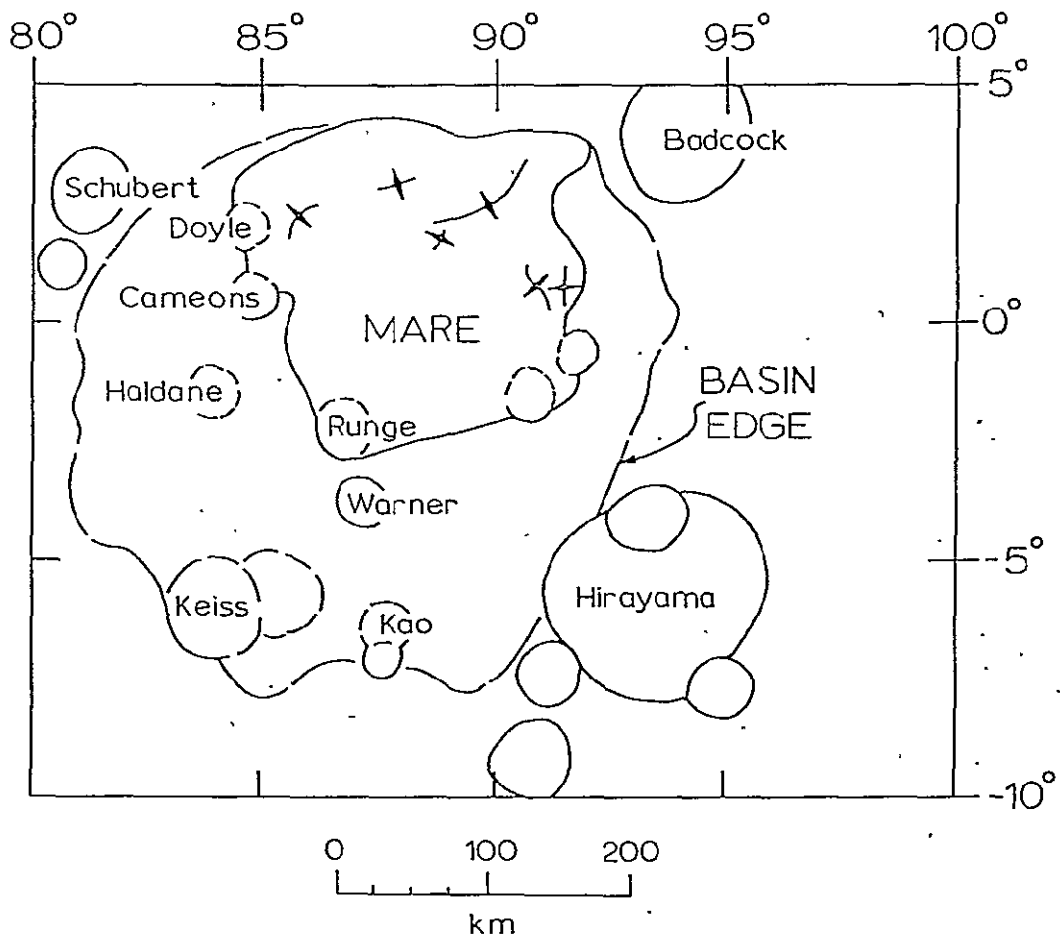


Figure 24

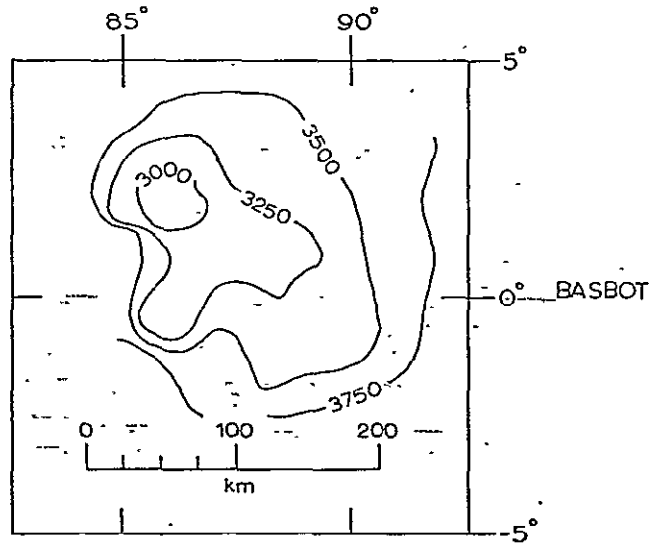
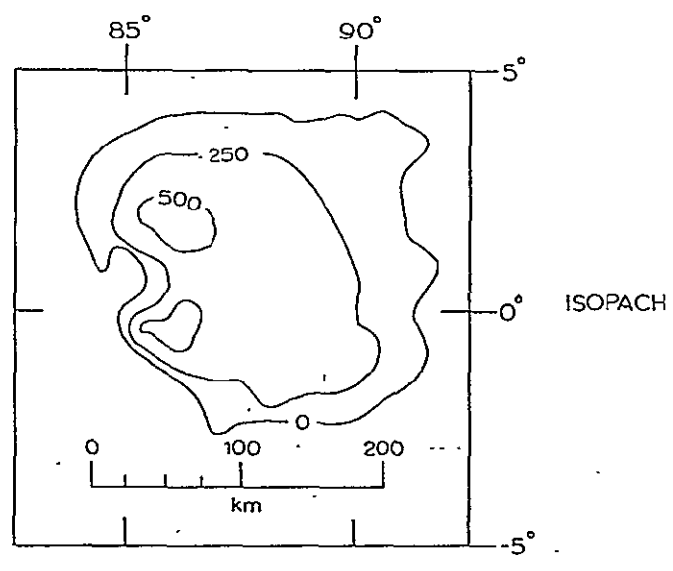
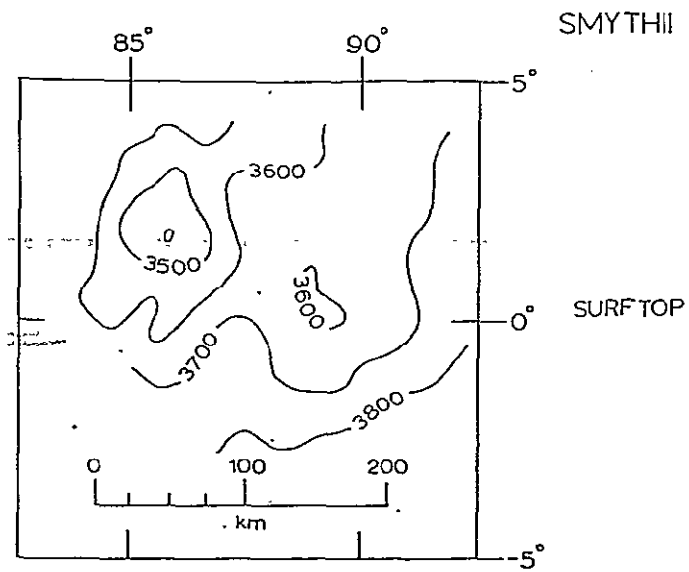


Figure 25

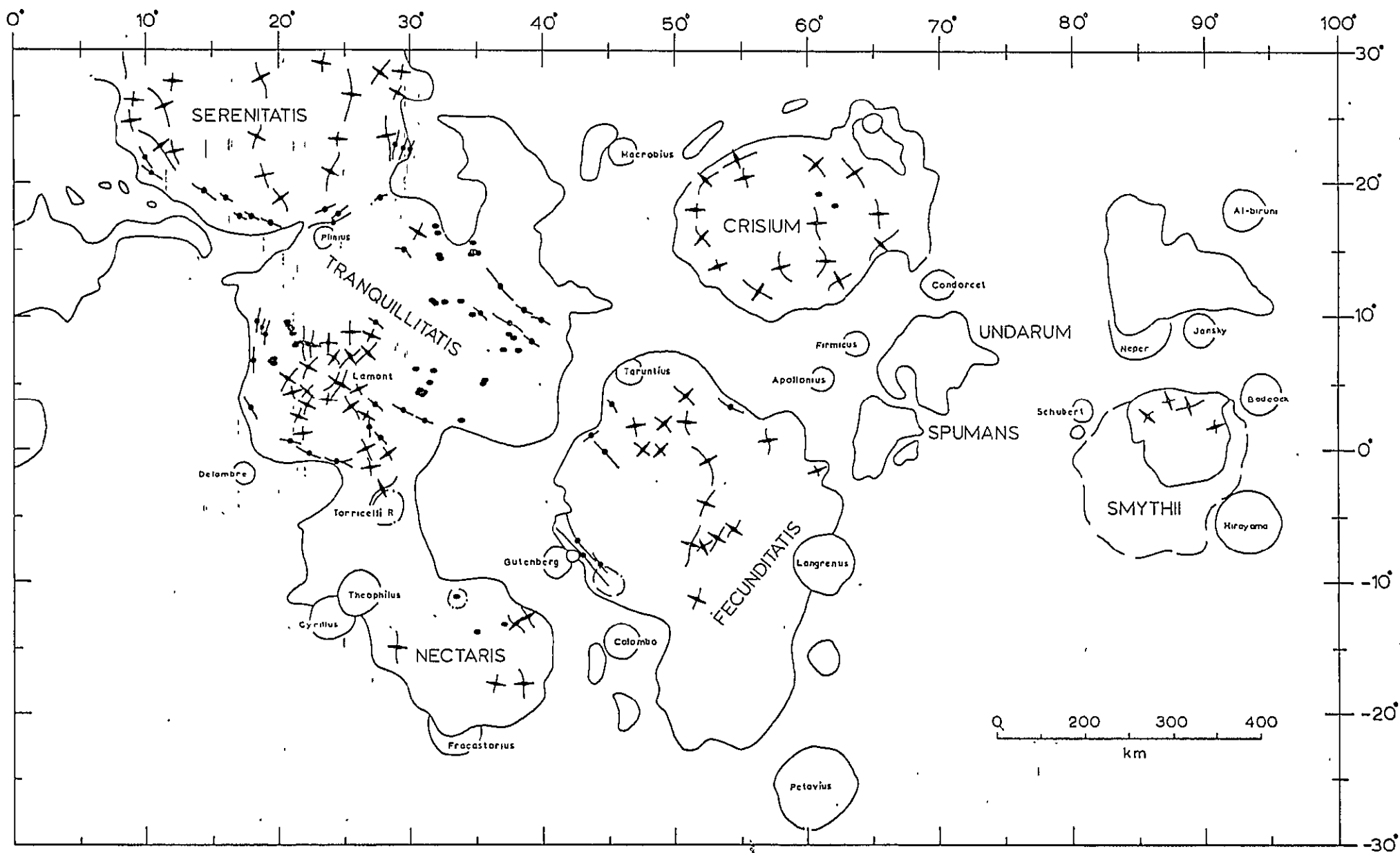


Figure 26

APPENDIX

Data Points used in Map Construction

Column 1	Latitude
Column 2	Longitude
Column 3	Basalt thickness
Column 4	Surface elevation (LTO base map)

<u>Basin</u>	<u>Page</u>
Mare Serenitatis	2
Mare Tranquillitatis and Sinus Amoris	3
Mare Nectaris	5
Mare Crisium	6
Mare Fecunditatis	7
Mare Spumans	9
Mare Undarum	10
Mare Smythii	11

MARK SERENTITATIS

23.5	20.25	150.	4700.
23.5	21.25	200.	4650.
22.0	28.75	678.	4600.
21.0	28.0	806.	4300.
18.0	23.5	380.	4450.
16.5	19.25	170.	4600.
16.1	23.0	60.	6000.
27.75	7.0	0.0	4800.
27.70	6.0	0.0	4850.
26.75	8.0	0.0	4800.
26.0	29.25	0.0	4700.
26.0	8.1	0.0	4800.
25.0	29.5	0.0	4600.
25.0	7.75	0.0	4750.
24.5	7.5	0.0	4750.
24.0	29.75	0.0	4650.
24.0	8.0	0.0	4750.
23.0	7.5	0.0	4900.
22.75	8.0	0.0	4850.
22.25	9.0	0.0	4800.
21.5	29.0	0.0	4500.
21.5	30.0	0.0	5000.
21.0	9.5	0.0	5100.
20.25	9.0	0.0	5200.
19.5	11.0	0.0	4900.
19.0	11.5	0.0	4900.
18.5	12.0	0.0	4950.
18.25	13.0	0.0	4950.
18.0	13.5	0.0	4900.
17.0	14.25	0.0	4800.
16.9	22.0	0.0	5100.
16.5	15.0	0.0	5000.
16.4	21.0	0.0	4900.
16.25	20.0	0.0	4600.
16.1	20.0	0.0	4650.
16.0	19.7	0.0	4500.
16.0	21.5	0.0	6050.
15.9	18.0	0.0	4650.
15.8	19.0	0.0	4550.
18.0	11.0	0.0	7000.
20.0	8.0	0.0	7200.
22.0	7.0	0.0	7000.
27.0	10.0		4600.
25.0	12.0		4700.
26.0	17.0		4650.
27.0	19.0		4900.
26.0	22.0		4650.
26.0	26.0		4500.
24.0	27.0		4375.
24.0	22.0		4600.

24.0	18.0	4650.
24.0	13.0	4740.
24.0	10.0	4650.
23.0	24.0	4475.
22.0	14.0	4680.
22.0	17.0	4700.
21.5	23.0	4475.
21.0	25.0	4475.
21.0	26.0	4400.
21.0	20.0	4575.
21.0	11.0	4800.
19.0	20.0	4650.
18.0	27.0	4900.
19.0	17.0	4800.
19.0	21.0	4700.
18.0	20.0	4600.
25.0	28.0	4370.
19.0	25.0	4400.
26.0	27.0	4380.

**ORIGINAL PAGE IS
OF POOR QUALITY**

MARF	TRANQUILLITATIS						
2.0	22.0	829.		12.7	38.5	620.	6400.
-2.0	29.5	946.		16.0	37.0	1000.	6200.
-2.5	27.0	1145.		20.0	28.25	0.0	4500.
22.5	38.0	90.	5900.	20.0	41.25	0.0	6100.
14.0	36.75	750.	6050.	14.0	28.75	0.0	5000.
12.5	37.5	526.	6200.	18.75	30.0	0.0	5400.
17.25	31.0	509.	5800.	17.25	40.5	0.0	6100.
16.25	29.25	225.	5700.	17.0	32.25	0.0	6000.
15.75	36.5	674.	6250.	16.0	32.5	0.0	6200.
15.25	28.75	807.	5700.	16.0	32.75	0.0	6400.
15.0	32.0	570.	6200.	15.5	34.5	0.0	7000.
14.75	29.25	350.	6000.	15.25	33.0	0.0	6400.
14.25	39.5	290.	6100.	15.0	33.75	0.0	6300.
14.25	20.25	205.	5950.	15.0	21.12	0.0	6200.
14.25	36.75	184.	6350.	14.75	20.0	0.0	6200.
14.25	38.5	150.	6200.	14.0	39.75	0.0	6200.
14.0	26.25	160.	5300.	14.0	19.25	0.0	5900.
13.6	30.7	970.	6200.	13.5	40.0	0.0	6050.
13.5	28.5	168.0	6100.	13.25	17.5	0.0	6100.
13.5	19.75	69.0	5600.	13.0	40.5	0.0	6100.
13.25	19.75	240.	5600.	13.0	18.25	0.0	5900.
12.25	29.75	460.	6250.	12.75	16.0	0.0	6900.
12.0	37.75	418.	6400.	12.5	41.0	0.0	6200.
11.6	21.8	400.	5600.	12.25	17.0	0.0	6400.
11.5	41.0	624.	6175.	12.25	16.0	0.0	6800.
11.0	41.0	472.	6250.	12.25	42.25	0.0	6200.
10.5	40.25	330.	6400.	12.0	41.75	0.0	6100.
10.0	40.25	205.	6500.	12.0	42.75	0.0	6200.
10.0	39.5	140.	6550.	12.0	43.5	0.0	6200.
6.8	40.5	400.	6500.	13.0	17.00	0.	
4.3	39.3	450.	6200.	11.0	16.75	0.	
11.0	27.8	1030.		10.0	17.50	0.	
10.8	20.2	700.		9.0	42.25	0.	
9.7	27.0	838.		9.0	18.00	0.	
8.5	29.0	817.		8.0	17.25	0.	
7.2	39.6	860.		7.0	17.75	0.	
6.7	34.6	886.		6.0	18.00	0.	
6.1	35.5	436.		5.0	17.50	0.	
5.0	32.8	946.		4.0	43.50	0.	
4.2	35.3	360.		4.0	17.00	0.	
5.0	24.5	1135.		3.0	17.25	0.	
6.0	22.8	1135.		3.0	41.50	0.	
3.8	23.0	1135.		11.25	44.0	0.0	6250.
3.5	25.0	858.		11.0	45.0	0.0	6250.
3.0	31.3	500.		10.6	45.5	0.0	6100.
2.6	32.6	746.		10.25	45.0	0.0	6250.
23.3	35.7	108.	5600.	10.0	43.0	0.0	6100.
22.9	35.7	150.	5600.	10.0	42.0	0.0	6400.
22.4	38.0	90.	5800.	8.5	42.0	0.0	6200.
21.6	39.4	54.	5900.	8.0	41.75	0.0	6500.
21.0	36.0	450.	5750.	7.0	42.75	0.0	6450.
20.0	36.3	150.	5800.	5.0	41.25	0.0	6100.
19.0	36.8	547.	6000.	2.0	18.00	0.	

ORIGINAL PAGE IS
OF POOR QUALITY

18.7	38.5	620.	6400.
16.0	37.0	1000.	6200.
2.0	41.5	0.0	6300.
1.0	18.00	0.	
1.0	32.50	0.	
1.0	35.00	0.	
1.0	41.0	0.0	6300.
0.	18.00	0.	
0.	32.50	0.	
0.	38.00	0.	
-1.0	21.50	0.	
-1.0	22.75	0.	
-1.0	22.50	0.	
-1.0	31.75	0.	
-2.0	24.75	0.	
-2.0	30.50	0.	
-3.0	25.00	0.	
-3.0	30.50	0.	
25.0	32.8	0.	5600.
24.8	35.0	0.	5300.
24.7	32.1	0.	5700.
24.6	34.0	0.	5400.
24.0	32.7	0.	5600.
24.0	37.8	0.	6000.
24.0	33.0	0.	5500.
23.5	34.0	0.	5300.
23.0	38.5	0.	5800.
23.0	34.2	0.	5800.
22.5	34.0	0.	5750.
22.0	39.3	0.	5900.
22.0	34.4	0.	5600.
21.5	40.0	0.	6000.
21.0	40.2	0.	6100.
21.0	34.0	0.	6100.
20.5	33.25	0.	6100.
20.0	33.6	0.	6100.
20.0	35.5	0.	5900.
20.0	40.5	0.	6100.
20.0	41.3	0.	6000.
19.0	41.75	0.	6100.
18.3	36.0	0.	6200.
18.0	41.25	0.	6000.
18.0	35.2	0.	6300.
17.1	40.0	0.	6200.
17.0	35.2	0.	6500.
16.5	39.3	0.	6500.
16.0	35.2	0.	6500.
16.0	40.0	0.	6400.
25.5	34.0	0.	6750.
25.0	32.0	0.	6300.
24.0	40.0	0.	7400.
22.0	33.0	0.	6700.
22.0	42.0	0.	6600.
20.0	43.0	0.	7000.
17.0	34.0	0.	7400.

17.0	42.0	0.	6800.
16.0	41.0	0.	7300.
11.0	46.0	0.0	6100.
9.0	43.0	0.0	6500.
15.0	16.0	0.0	6800.
15.0	19.0	0.0	6700.
15.0	43.0	0.0	6500.

ORIGINAL PAGE IS
OF POOR QUALITY

DATE	NECTARIS	DATA CARDS					
-4.0	30.0	484.		-10.5	22.0	0.	5500.
-4.1	29.0	718.	5200.	-11.0	20.9	0.	6500.
-4.75	26.9	1218.	5000.	-11.0	37.2	0.	5100.
-5.4	23.8	538.	5000.	-11.6	20.7	0.	6800.
-5.4	25.0	721.	5200.	-12.0	25.0	0.	
-6.0	29.2	900.	5000.	-12.0	38.5	0.	
-6.2	25.1	652.	5350.	-13.0	40.25	0.	
-6.4	27.3	1100.	5000.	-14.0	27.0	0.	
-7.75	23.2	278.	5200.	-14.0	39.5	0.	
-8.0	26.0	226.	5100.	-14.0	40.0	0.	
-10.0	30.6	858.	5450.	-14.0	40.7	0.	
-10.7	32.4	807.	5000.	-15.0	39.5	0.	
-11.1	33.4	855.	4900.	-15.0	40.25	0.	
-11.8	36.8	754.		-15.0	40.75	0.	
-12.5	33.8	985.		-16.0	27.0	0.	
-12.6	38.5	748.		-16.0	39.7	0.	
-13.0	39.4	548.		-16.0	40.4	0.	
-14.0	32.0	3000.		-16.0	41.0	0.	
-14.0	37.4	678.		-17.0	29.0	0.	
-16.5	34.9	784.		-17.0	40.6	0.	
-17.6	37.6	348.		-18.0	30.0	0.	
				-18.0	40.0	0.	
				-19.0	30.0	0.	
-5.0	21.0	0.	6000.	-19.0	40.5	0.	
-5.0	32.0	0.	5900.	-20.0	31.5	0.	
-6.0	21.0	0.	7200.	-20.0	39.0	0.	
-7.0	21.0	0.	7600.	-21.0	32.0	0.	
-7.0	34.0	0.	7300.	-21.0	34.75	0.	
-8.0	21.0	0.	7800.	-21.0	36.0	0.	
-8.5	32.5	0.	6200.				
-8.5	34.5	0.	8200.	-5.25	29.1		5000.
-8.5	36.0	0.	5400.				
-9.0	21.0	0.	9400.				
-9.0	37.0	0.	6200.				
-10.0	20.0	0.	9600.				
-4.0	24.0	0.	5400.				
-4.0	30.8	0.	5450.				
-5.0	23.0	0.	5200.				
-5.0	30.7	0.	5450.				
-6.0	21.5	0.	5500.				
-6.0	22.0	0.	5500.				
-6.6	22.0	0.	5500.				
-8.0	22.0	0.	5200.				
-8.0	31.7	0.	5100.				
-9.0	22.1	0.	5100.				
-9.0	32.0	0.	4900.				
-10.0	22.25	0.	5100.				
-10.0	32.0	0.	5200.				
-10.0	33.0	0.	5100.				
-10.0	35.0	0.	5000.				
-10.0	36.0	0.	5200.				
-10.1	34.0	0.	5000.				
-10.1	37.0	0.	5400.				

ORIGINAL PAGE IS
OF POOR QUALITY

MARF	CRISIUM						
17.75	50.25	275.	4000.	10.0	54.0	0.0	8400.
14.8	52.3	800.	3800.	10.0	62.0	0.0	6000.
14.6	51.7	387.	3775.	9.0	55.0	0.0	6500.
13.5	63.2	569.	3700.	9.0	58.0	0.0	7000.
12.8	53.0	527.	3750.	9.0	60.0	0.0	6600.
11.5	54.25	230.	3700.	9.0	61.0	0.0	8000.
11.0	54.0	80.	3700.	9.0	63.0	0.0	5700.
11.0	58.75	370.	3500.	20.0	53.0		3675.
10.25	57.5	510.	3800.	20.0	55.0		3775.
				20.0	60.0		3650.
20.0	51.5	0.0	4200.	19.0	57.0		3800.
19.0	50.75	0.0	3950.	18.0	54.0		3750.
18.0	50.0	0.0	4000.	17.0	59.0		3640.
17.0	50.25	0.0	4000.	17.0	55.0		3650.
16.0	50.0	0.0	3900.	16.0	54.0		3625.
14.55	66.0	0.0	4000.	16.0	58.0		3800.
14.5	67.0	0.0	3900.	16.0	62.0		3625.
14.4	50.0	0.0	3700.	15.0	63.0		3625.
14.2	65.0	0.0	4000.	15.0	66.0		3825.
14.0	67.9	0.0	4000.	14.0	57.0		3600.
14.0	69.0	0.0	4000.	14.0	60.0		3480.
13.7	51.0	0.0	3800.	13.0	55.0		3525.
13.0	64.8	0.0	3800.	13.0	61.0		3460.
13.0	67.4	0.0	4200.	13.0	64.0		3900.
13.0	68.3	0.0	4300.	12.0	56.0		3600.
12.5	52.0	0.0	4000.	12.0	59.0		3475.
12.3	64.0	0.0	3800.	12.0	60.0		3380.
12.0	52.5	0.0	3800.	12.0	62.0		3650.
12.0	63.75	0.0	3900.				
11.75	53.5	0.0	3800.				
11.2	63.0	0.0	3900.				
10.9	61.5	0.0	3600.				
10.75	54.0	0.0	3750.				
10.6	62.4	0.0	3800.				
10.5	55.0	0.0	3750.				
10.5	59.0	0.0	3900.				
10.0	55.75	0.0	3700.				
10.0	58.25	0.0	4000.				
10.0	60.5	0.0	3900.				
9.5	57.75	0.0	4000.				
9.0	57.0	0.0	3700.				
20.0	50.0	0.0	8000.				
17.0	49.5	0.0	7700.				
14.0	66.0	0.0	8000.				
13.0	51.0	0.0	7300.				
13.0	66.0	0.0	6200.				
13.0	69.0	0.0	6800.				
12.0	52.0	0.0	6500.				
12.0	65.0	0.0	7500.				
11.0	53.0	0.0	6500.				
11.0	64.5	0.0	6900.				
10.0	52.0	0.0	7000.				

ORIGINAL PAGE IS OF POOR QUALITY

MARE	FECUNDITATIS			-17.6	49.6	60.	
5.5	49.0	377.	5000.				
5.5	50.0	218.	5050.	7.0	50.5	0.0	5100.
4.5	50.0	275.	5100.	6.0	52.0	0.0	5200.
4.5	49.75	443.	5000.	5.0	45.0	0.0	5700.
4.0	46.75	205.	5250.	4.0	44.6	0.0	5500.
3.75	49.75	571.	4750.	4.0	53.5	0.0	5150.
3.25	47.5	366.	5100.	3.75	54.0	0.0	5400.
2.9	55.3	100.	5200.	3.0	44.7	0.0	5600.
2.4	53.75	210.	5000.	3.0	55.0	0.0	5200.
2.25	54.3	200.	5000.	2.75	59.0	0.0	4700.
2.0	52.5		4950.	2.75	58.0	0.0	4800.
1.8	59.4	108.	4900.	2.25	52.0	0.0	5500.
1.7	57.8	946.	4750.	2.5	56.0	0.0	5250.
1.3	55.85	85.	5100.	2.0	44.6	0.0	5500.
1.2	58.6	136.	4900.	2.0	56.75	0.0	5200.
0.9	43.7	100.	6100.	2.0	59.5	0.0	4900.
-0.5	57.0	439.	5000.	2.0	56.25	0.0	5350.
-0.5	54.75	303.	4610.	1.25	44.0	0.0	6050.
-0.6	42.5	500.	6000.	1.25	59.75	0.0	5000.
-0.75	58.25	178.	5400.	1.0	58.25	0.0	4800.
-0.75	49.5	693.	5500.	1.0	42.75	0.0	6050.
-0.9	61.2	100.	5400.	0.25	59.0	0.0	5250.
-1.1	61.2	200.	5350.	0.0	42.25	0.0	6000.
-1.25	60.0	296.	5400.	0.0	59.5	0.0	5500.
-1.3	43.1	750.	5920.	-0.5	42.0	0.0	6150.
-1.4	60.9	160.	5450.	-0.75	61.0	0.0	5450.
-1.75	56.75	255.	5250.	-1.0	61.5	0.0	5400.
-2.0	50.0	1450.	5375.	-1.0	60.0	0.0	5400.
-2.25	59.5	296.	5200.	-1.75	61.5	0.0	5300.
-2.3	60.2	227.	5350.	-2.0	61.0	0.0	5500.
-2.6	41.9	370.	5850.	-2.0	41.0	0.0	5500.
-2.7	60.9	150.	5400.	-2.8	41.0	0.0	5200.
-3.0	44.3	745.	5600.	-3.0	42.0	0.0	5700.
-3.0	56.25	200.	5200.	-3.0	61.0	0.0	5350.
-3.4	60.5	210.	5050.	-3.0	62.0	0.0	5200.
-3.5	56.0	114.	5400.	-4.0	41.5	0.0	5900.
-3.8	41.8	490.	5700.	-4.5	42.5	0.0	5700.
-4.0	60.8	150.	5150.	-5.0	42.5	0.0	5700.
-4.0	61.5	450.	5200.	-5.0	41.0	0.0	5500.
-5.75	55.75	351.	5400.	-5.5	41.0	0.0	5600.
-5.9	52.3	670.	5200.	-6.0	40.75	0.0	5700.
-5.9	45.	380.	5750.	-6.5	41.0	0.0	5600.
-6.0	57.0	276.	5500.	-8.0	61.0	0.	
-6.0	53.8	340.	5340.	-9.00	43.25	0.	
-6.6	43.	325.	5550.	-10.0	60.5	0.	
-7.5	54.2	550.	5225.	-10.00	43.00	0.	
-7.9	49.9	807.	5700.	-11.00	44.00	0.0	
-8.0	42.9	408.	5600.	-12.0	60.0	0.	
-8.2	49.4	748.		-13.0	49.0	0.	
-8.6	45.6	921.		-13.00	59.75	0.	
-9.4	50.2	720.		-14.0	49.5	0.	
-12.4	53.1	600.		-14.00	59.00	0.	
-14.8	53.2	153.		-15.00	58.75	0.	

ORIGINAL PAGE IS
OF POOR QUALITY

-15.0	49.25	0.
-16.00	48.75	0.
-17.00	48.50	0.
-18.00	59.00	0.
-18.0	48.75	0.
-19.00	48.25	0.
-20.00	49.25	0.
-20.00	58.00	0.
-22.00	52.50	0.
-21.0	49.75	0.
-22.00	49.75	0.
-22.0	53.75	0.
-22.50	59.50	0.
-23.00	51.00	0.
-22.50	51.75	0.
-23.0	55.00	0.

7.0	52.0	0.0	5500.
7.0	47.0	0.0	5350.
7.0	54.0	0.0	7100.
6.0	54.0	0.0	5800.
5.0	54.0	0.0	5100.
4.0	44.0	0.0	6400.
3.5	56.0	0.0	5800.
3.5	58.0	0.0	5500.
3.0	44.0	0.0	6300.
3.0	60.0	0.0	5650.
3.0	43.0	0.0	6850.
2.0	60.0	0.0	5000.
2.0	42.0	0.0	6250.
2.0	43.0	0.0	6000.
1.0	42.0	0.0	5950.
0.0	60.0	0.0	5400.
-0.5	41.0	0.0	6000.
-1.0	62.0	0.0	6000.
-1.0	41.0	0.0	6500.
-2.0	63.0	0.0	6000.
-2.5	40.0	0.0	5600.
-4.0	64.0	0.0	6000.
-4.4	40.8	0.0	6500.
-6.0	40.0	0.0	5800.
-8.0	40.0	0.0	6400.
-5.0	47.0		5175.

ORIGINAL PAGE IS
OF POOR QUALITY

MARE SPUMANS							
3.7	65.2	200.	5600.	0.8	68.3	0.0	5900.
2.8	65.3	195.	5400.	0.7	68.9	0.0	6750.
2.7	67.7	259.	6500.	0.5	66.5	0.0	5800.
2.5	66.4	340.	5400.	0.5	63.4	0.0	5500.
2.4	67.8	303.	6500.	0.5	68.0	0.0	5750.
2.2	67.0	425.	6400.	0.5	68.3	0.0	5800.
1.5	67.2	286.	5550.	3.0	63.0	0.0	6300.
1.5	65.5	150.	5400.	2.0	63.0	0.0	5500.
1.4	64.7	294.	5500.	1.0	62.0	0.0	5300.
1.0	66.7	377.	5500.	0.1	66.9	0.0	8400.
0.8	64.1	453.	5700.	0.0	62.5	0.0	5700.
-0.2	64.0	350.	5900.	-0.3	64.3	0.0	6723.
-0.5	67.5	100.		-1.5	63.0	0.0	6000.
-0.5	64.5	450.	5900.	-1.5	64.8	0.0	7310.
-0.6	64.0	810.	5370.	-2.5	63.5	0.0	6000.
-1.0	63.9	700.	5600.				
-1.9	64.2	540.	5600.				
0.0	67.2	0.0	5700.				
0.0	68.4	0.0	5600.				
0.0	63.4	0.0	5700.				
-0.3	63.8	0.0	5600.				
-0.5	66.3	0.0					
-0.5	66.7	0.0					
-0.5	67.0	0.0					
-0.6	68.4	0.0					
-0.7	67.3	0.0					
-0.8	68.0	0.0					
-1.0	66.4	0.0					
-1.0	63.5	0.0	5700.				
-1.0	65.7	0.0					
-1.2	67.0	0.0					
-1.3	66.7	0.0					
-1.5	65.5	0.0					
-1.5	63.5	0.0	5700.				
-2.0	65.6	0.0					
-2.2	64.5	0.0	5900.				
-2.4	64.0	0.0	5500.				
-2.4	65.0	0.0	5850.				
-2.5	65.3	0.0	5800.				
4.0	65.6	0.0	5700.				
3.1	66.0	0.0	5500.				
3.0	68.0	0.0	6500.				
3.0	67.5	0.0	6500.				
3.0	67.1	0.0	6300.				
3.0	66.5	0.0	6200.				
3.0	64.0	0.0	5500.				
2.0	63.9	0.0	5500.				
2.0	68.0	0.0	6600.				
1.0	69.0	0.0	6600.				
1.0	63.8	0.0	5500.				
1.0	68.5	0.0	6600.				
0.8	67.6	0.0	6600.				

ORIGINAL PAGE IS
OF POOR QUALITY

MARF	SMYTHII		
4.25	87.0	145.	3450.
2.6	88.6	320.	3700.
2.0	85.75	550.	3400.
1.0	89.25	375.	3600.
-0.25	89.75	275.	3600.
-0.5	86.0	635.	3600.
-1.0	90.25	330.	3700.
-1.25	87.50	265.	3800.
-1.50	88.50	355.	3700.
4.5	88.0	0.0	3500.
4.4	87.0	0.0	3500.
4.2	91.0	0.0	3650.
4.1	86.0	0.0	3550.
4.1	90.0	0.0	3650.
4.0	89.0	0.0	3500.
4.0	91.7	0.0	3650.
3.5	92.0	0.0	3750.
3.0	84.2	0.0	3700.
3.0	91.3	0.0	3650.
2.0	91.4	0.0	3700.
1.0	84.6	0.0	3600.
1.0	92.0	0.0	3750.
0.7	85.6	0.0	3600.
0.4	84.5	0.0	3550.
0.2	85.5	0.0	3600.
0.0	91.5	0.0	3700.
-1.0	85.5	0.0	3700.
-1.3	91.8	0.0	3750.
-1.5	86.0	0.0	3700.
-2.0	91.0	0.0	3700.
-2.5	89.0	0.0	3750.
-2.7	88.0	0.0	3700.
-3.0	87.0	0.0	3700.

ORIGINAL PAGE IS
OF POOR QUALITY